11. Chemistry in Clusters: Solvation at the Single Molecule Level

JACK A. SYAGE
The Aerospace Corporation, P.O. Box 92957/M5-754, Los Angeles, CA 90009, U.S.A.

1. Introduction

One of the more familiar statements made about clusters is that they represent a phase of matter than is neither gas phase nor condensed phase, but somewhere in between. If so, then it is reasonable to expect that the physical and chemical behavior of clusters should take on properties that are intermediate between gas phase and condensed phase properties. The impetus to cluster research is driven largely by the potential to learn about the correspondence between these conventional phases of matter and the hope that some unforeseen molecular level properties of the condensed phase will be revealed in the cluster environment.

Research in clusters is pursued in a wide variety of scientific disciplines, including atomic physics (condensation, electron shell structure), laser physics (excimers), material science (crystal growth, phase transitions), chemistry (microsolvation, catalysis), and biochemistry (site-selective bonding, enzyme activity) [1, 2]. Our particular interest is in chemical reactivity in clusters and the dynamical events (energy redistribution, bond rearrangement, solvent reorganization) that accompany chemistry. The chemistry that we will discuss is initiated by a photoexcitation or photoionization pulse and the evolution of cluster properties are interrogated at later times by various probe excitation and detection techniques. The classes of chemistry in clusters reviewed here include ion-molecule reactions (e.g. electron and proton transfer, and sigmatropic rearrangements) [3–11], neutral excited-state proton transfer [11–18], and free radical chemistry [19].

The most common method of producing clusters is by supersonic expansion. This process gives rise to molecular cooling and low-energy collisions that promote cluster growth [20]. The cold clusters are formed nearly exclusively in their vibrationless level with rotational energy that is negligible on a chemical-energy scale. Photoexcitation energy can account for a large fraction of the total cluster internal energy. These experimental conditions allow important properties of the clusters to be selectively controlled, making them ideally suited as molecular-level models of the condensed phase.

J.D. Simon (ed.), Ultrafast Dynamics of Chemical Systems, 289–326.

4.3 "HOT" RADICAL REACTION MECHANISM

The 266 nm picosecond mass spectra in Figures 9d and 11 show that the photoexcited clusters can lose a substantial fraction of the CH_3 groups allowable by cluster size. Also evident in Figure 11 is an alternation of peak intensities separated by two CH_3 mass units. Because the product distribution is observed to shift to greater demethylation at higher pulse energies, it is believed that sequential photon absorption plays some role in demethylation. However, because demethylation is relatively extensive even at low pulse energies (Figure 11b), it seems unlikely that sequential photon absorption can account for all the products observed. This conclusion is supported by the photon flux and absorption cross section data [19].

The picosecond measurements and mass spectral features can be explained by a simple, but not necessarily unique, reaction mechanism based on the chemistry of a "hot" CH_3 radical. The photodissociation of CH_3I by 266 nm light provides a 4.66 eV photon to break the 2.30 eV C—I bond. The excess energy in the direct dissociation is released mainly as kinetic energy in the CH_3 radical [57], which can lead to the exothermic reaction

$$[CH_3 + (CH_3I)_{n-1}] \longrightarrow C_2H_6 + I(CH_3I)_{n-2} \qquad \Delta H = -1.37 \text{ eV}$$

where we assume that the photodissociated I atom is lost (recombination of I atoms would contribute an additional exothermicity of $\Delta H = -1.58$ eV). An alternative pathway to production of ethane would involve the absorption of two photons by $(CH_3I)_n$ to produce two CH_3 radicals that could recombine to release 3.81 eV of heat. In both cases the heat of reaction, which is augmented by the initial radical kinetic energy as well as further recombination including the dissociated I atoms, could drive additional chemistry based on the exothermicity of ethane formation. The hot cluster product above, for example, could undergo the thermal rearrangement

$$I(CH_3I)_{n-2} \longrightarrow C_2H_6 + I_3(CH_3I)_{n-4} \qquad \Delta H = -0.52 \text{ eV}$$

with the additional heat sustaining further loss of ethane. Again subsequent photodissociation would enhance the rate of C—I bond breaking and exothermic production of C_2H_6.

The near absence of a multiple I atom loss product is consistent with efficient caging of this heavy mass which acquires little kinetic energy (0.15–0.25 eV) by photodissociation and even less by the thermal route. This provides an efficient means for production of the major product I_2. Recent work by Ziegler *et al.* [55] and Fan and Donaldson [56] show that on the nanosecond timescale thermally hot I_2 is observed free of the clusters (although the excitation energy and, therefore, the I_2 energy content differ in these two studies). It will be interesting in a future time-resolved experiment

to measure the rate of production of I_2 in the cluster and the subsequent rate of evaporation or separation from the cluster. Perhaps I_2 in different vibrational levels will show different time dependences reflecting some diversity of the local environment in clusters.

5. Ion-Molecule Chemistry

5.1 Deciphering Gas-Phase Reaction Coordinates

Large compilations of data now exist for gas-phase bimolecular ion-molecule reactions. The most common and routine properties measured in gas-phase experiments are product branching ratios, enthalpies, and activation energies. Much less information is obtained regarding the reactive complex in terms of structure, minima energy, and boundness. Rather these properties are inferred from thermodynamic and kinetic data or from theory, and are often represented by a reaction coordinate for the minimum energy path to products. Although, the minimum energy path is the most probable route for product formation, it is not the most likely owing to the random nature of collision-pair impact parameter and orientation. However, determining a multidimensional potential energy surface encompassing a large gamut of collision parameters is not feasible except for the simplest reactions (e.g., atom-diatom reactions). Cluster research, however, can provide crucial information.

Photoexcitation of van der Waals (vdW) complexes is a useful way to study the bound and quasibound reactive complexes associated with gas-phase bimolecular collisions [58, 59]. Ionization of vdW complexes to form reactive complexes of ion-molecule reactions [3–11] is especially favorable because they tend to be stable due to charge-induced dipole interactions. These complexes assume the lowest energy structure and so can be expected to be typical of the minimum energy reaction coordinate of a bimolecular reaction. At any rate, a van der Waals complex represents a single coordinate; in other words an aligned complex.

Ion-molecule kineticists, for many years, have postulated that some reactions (mostly fast) proceed along barrierless single-well reaction coordinates whereas other reactions (mostly slow) involve double-well barrier processes [60]. Included in the latter group were classes of reactions in which the charge distribution in the reactant was delocalized from the eventual charged leaving group (as can happen in electron and proton transfer reactions and S_n2 substitutions [62]). The double-minima barrier mechanism [60, 61] became widely accepted well before the existence of two distinct and stable reactive complexes was experimentally confirmed [10, 11]. $PhOH^+$ is an acid cation that has a ground electronic-state charge distribution delocalized from the poten-

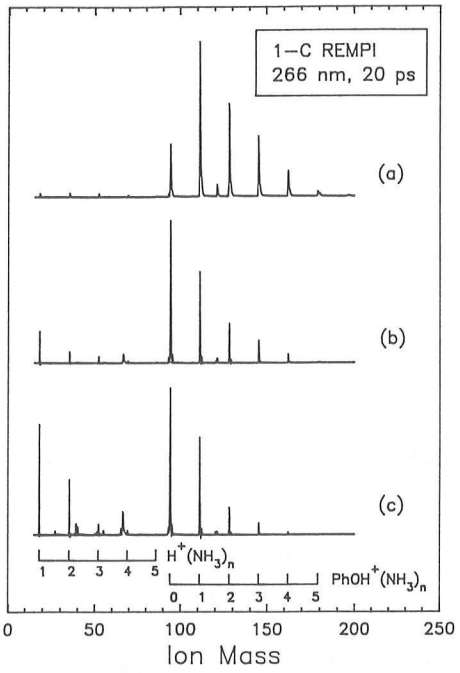

Fig. 12. One-color picosecond REMPI mass spectra as a function of increasing pulse energy. (a) two-photon signals, (b) appearance of $H^+(NH_3)_n$ at the three-photon level, (c) appearance of aromatic fragmentation at the four-plus photon level.

tial proton leaving group, which prompted us to investigate the possibility of detecting two stable complex forms for the reaction

$$PhOH^+ + (NH_3)_n \longrightarrow PhO + H^+(NH_3)_n$$

Using a picosecond delayed-ionization technique, we determined that there are two stable reaction complexes: $PhOH^+ \cdots (NH_3)_n$ and $PhO \cdots H^+(NH_3)_n$. By referring to Figure 2, it can be seen that zero time-delay pump-probe ionization forms complex ions of the first type. These are strongly bound to proton transfer as seen by the lack of $H^+(NH_3)_n$ in the picosecond two-photon ionization mass spectrum in Figure 12a. Only by increasing pulse energy so that the ion complex absorbs a photon was the barrier surmounted to produce $H^+(NH_3)_n$ (Figures 12b and 12c). The product complex can be formed by taking advantage of the ESPT reaction from S_1 phenol and using delayed ionization, as shown in Figure 2. This ion complex, being formed on the product side of the barrier, readily dissociates to $H^+(NH_3)_n$ as seen in Figure 13. For high energy ionization (two 532-nm photons), the second complex was observed to be 95% dissociative [11]. Witness the decay of $PhOH^+(NH_3)_n$ signal to near zero for 532-nm ioniza-

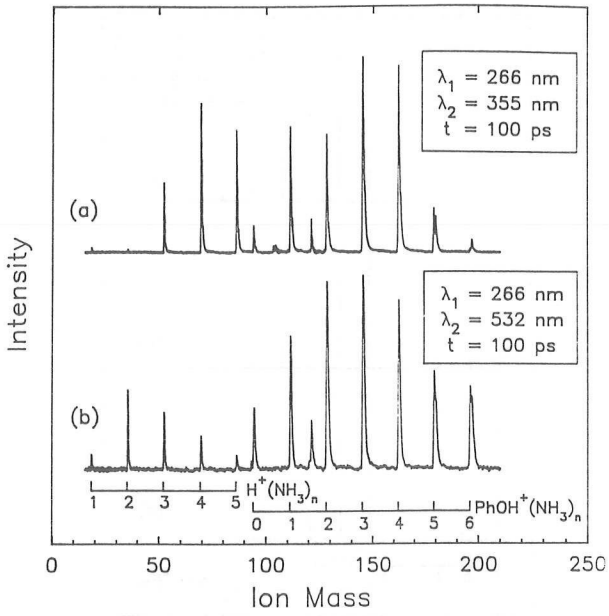

Fig. 13. Two-color picosecond delayed ionization REMPI mass spectra for (a) $\lambda_2 = 355$-nm, one-photon ionization, and (b) $\lambda_2 = 532$-nm, two-photon ionization.

tion (Figures 3 and 14a). For lower energy ionization (one 355-nm photon), the $PhOH^+(NH_3)_n$ signal decays to a plateau level corresponding to 65% dissociation (Figure 14b) [11]. Because at later times the signal is due to the $PhO \cdots H^+(NH_3)_n$ complex, we can conclude that it is bound and stable.

What was uncertain from our earlier work was the height of the barrier because we did not know the distribution of ion energies. This measurement has since been made by photoelectron spectroscopy. Figure 15 shows the PES for different photon energies. A distribution of cluster sizes is ionized, all of which contribute to the PES. The maximum electron energy for each cluster size is marked, based on reported ionization potentials [16]. Figure 15a corresponds to the photoelectron spectrum for cluster sizes $n > 4$, achieved by using an excitation wavelength of 286 nm that is to the red of the $S_1 \leftarrow S_0$ origin transition for the smaller cluster sizes [16]. The energy distribution for these larger complexes extends to relatively high energy. Similar results are seen for the other spectra. The spectra in Figures 15d and 15e demonstrate that the cluster ions for $n = 1$ and 2 are also formed with substantial energy. These spectra compare the results for a large cluster distribution (not greatly exceeding $n = 6$) produced by ionization in the cold central portion of the gas pulse (Figure 15d) and for a small cluster distribution (dominated by $n \leq 3$) produced by ionization resonant with $n = 1$ in the warm leading edge of the

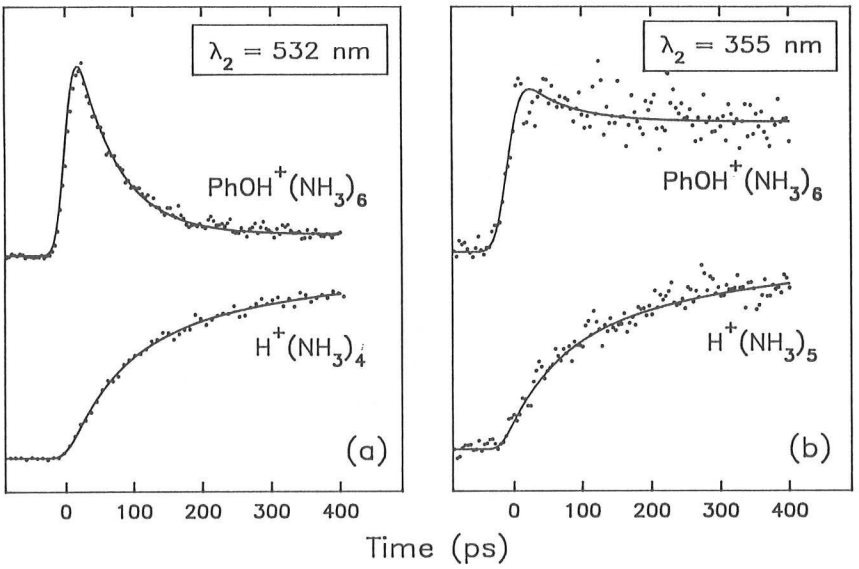

Fig. 14. Time-resolved measurements of reactant and product ionization signals $[PhOH]^+ \cdot (NH_3)_n$ and $H^+(NH_3)_n$, respectively, for cluster size $n = 6$. (a) $\lambda_2 = 532$-nm, two-photon ionization, (b) $\lambda_2 = 355$-nm, one-photon ionization. We show $H^+(NH_3)_4$ traces for $n = 4$ and $n = 5$ because, typically, two and one solvent molecules evaporate at these respective ionization energies following dissociative proton transfer [19b]. The calculated curves were fitted to a model in Ref. 10 for rate constants of $k = (65\ \text{ps})^{-1}$ and $k_s = (350\ \text{ps})^{-1}$ and proton dissociation fractions for the product ion of 100% for 532-nm ionization and 65% for 355-nm ionization. The reactant ion is essentially undissociated.

gas pulse (Figure 15e). The latter spectrum shows that the energy distribution in these cluster ions extends to high energy.

Despite the congested spectra, it is possible to see that a fairly large fraction of ions are formed with energies greater than 1 eV. Yet these complex ions are known to be stable to proton dissociation according to the mass spectra in Figure 12. These results would argue that the ion-molecule proton transfer reaction above (at least for small n) has a barrier of at least 1 eV. The model for the potential energy surface, discussed below, sets an upper limit for the barrier of 1.5 eV.

Potential Energy Curve and Reaction Coordinate: We review the general features of a potential energy model for delocalized charge transfer described in detail elsewhere [10, 11]. The model proposed for the potential energy surface and reaction coordinate is pictured in Figure 16. Potential energy curves along the O—H coordinate are drawn for isolated $[PhOH]^+$ (back panel) and for $[PhOH \cdot NH_3]^+$ (front panel). The N—H coordinate running from back to front represents the approach of reactants in a bimolecular reaction and the O—H coordinate, just mentioned, represents departure of products.

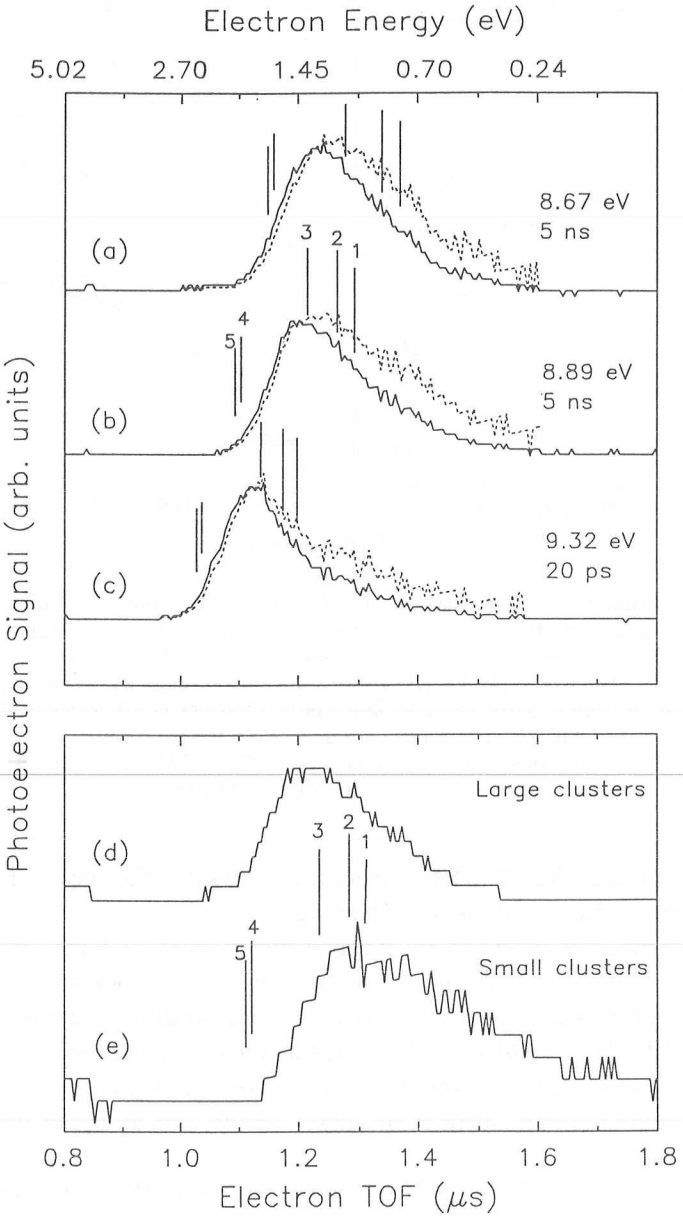

Fig. 15. Photoelectron spectra for resonance two-photon ionization of $PhOH \cdot (NH_3)_n$ clusters. (a) 286-nm excitation, $n_{max} \sim 4 - 5$; (b) 279-nm excitation, $n_{max} \sim 3$; (c) 266-nm excitation, $n_{max} \sim 3 - 4$; (d) 280-nm excitation at center of gas pulse, $n_{max} \sim 4$; (e) 280-nm excitation at edge of gas pulse, $n_{max} \sim 2$. The n_{max} values are estimated from mass spectra and knowledge of cluster $S_0 \leftarrow S_1$ transition energies. The vertical lines represent IPs for clusters of size n. The dotted curves in (a)–(c) are corrected for electron kinetic energy detection efficiency.

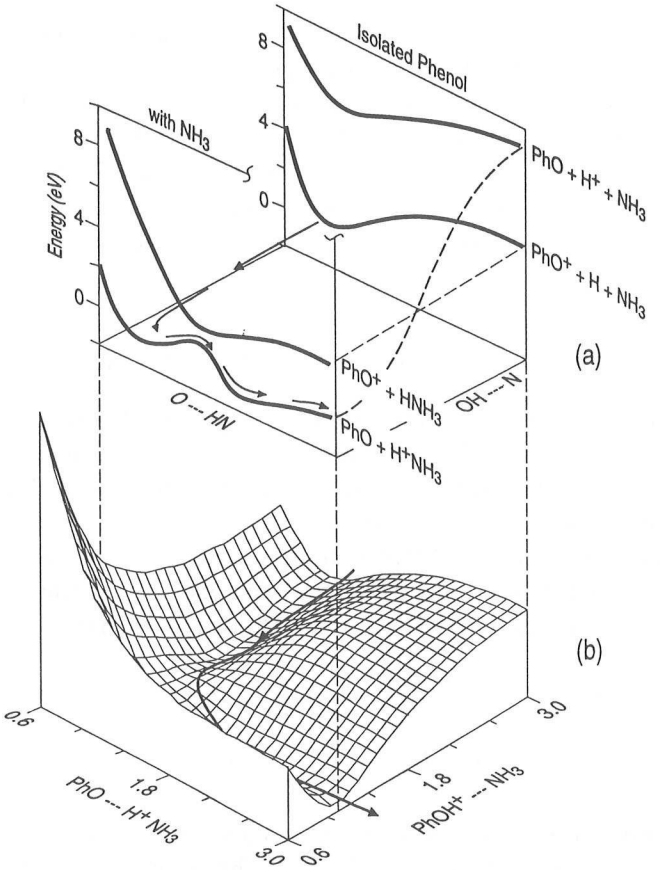

Fig. 16. Model of the potential energy reaction coordinate for the reaction $PhOH^+ + NH_3 \longrightarrow PhO + NH_4^+$. (a) Potential energy curves for uncomplexed and complexed $PhOH^+$ showing the surface crossing that gives rise to the barrier to proton transfer. (b) A rendition of the lower adiabatic potential energy surface for the collinear O···H···N coordinate (in Å). Reaction paths are drawn for visualization in (a) and (b).

The reaction coordinate is approximated by the path marked by arrows. The barrier is predicted on the basis of a simple concept. The ground electronic state of $PhOH^+$ dissociates to $PhO^+ + H$. The dissociative limit for $PhO + H^+$ is about 5 eV higher in energy (given by the difference in the ionization potentials of PhO and H, 8.56 and 13.60 eV, respectively) [63] and is probably associated with some higher unknown excited electronic state of $PhOH^+$. This dissociative limit is stabilized enormously as NH_3 approaches along the N—H coordinate because of the substantial 8.86 eV proton affinity [39] of NH_3. Because the ground state dissociative limit $PhO^+ + H$ experiences considerably less stabilization from NH_3, the dissociative limits are reversed in

energy by the approach of reactant NH_3 (dotted lines, Figure 16a). This causes a surface crossing that creates the barrier to reaction. The surface crossing reaction barrier should be a general property of reactions in which the charged leaving group is not the lowest energy dissociative limit of the isolated ion. And this situation will be typical of ions where charge is delocalized from the leaving group. A visualization of the shape of the lower adiabatic surface for the collinear O $\cdots$ H $\cdots$ N coordinate is given in Figure 16b [10, 11]. The reaction path drawn represents the lowest energy reaction coordinate in the classical limit (ignoring zero-point energy).

5.2 ELECTRON TRANSFER INDUCED BY DISSOCIATION

All chemistry defined by transformation of chemical bonds involves charge transfer in some form of interpretation. Thermodynamically driven reactions seek products that minimize electronic energy. Changes in electronic energy are brought about by redistribution of charges and occur in both the gas phase and solution phase. Many common reactions in solution phase involve transfer of relatively localized charges from one group to another. Two good examples are S_n2 and proton transfer (PT) reactions [64], as shown below

$$X^- + RY \longrightarrow XR + Y^- \qquad (S_n2)$$

$$AH^+ + B \longrightarrow A + BH^+ \qquad (PT)$$

The stability of charge reactions are usually strongly dependent on solvent properties (i.e., polarity, proton affinity). The above classes of reactions also occur in the gas-phase; however, their stability is greatly affected by the absence of solvent. The role of electron or charge transfer is obviously of great importance to chemistry, so we will open up the discussion somewhat to consider non-chemical electron transfer processes. (We define electron transfer (ET) as the specific case of charge transfer involving increments of unit charge.) Two examples of the latter processes in the gas phase are collisional charge transfer (CT) and Penning ionization, shown below

$$A^+ + B \longrightarrow A + B^+ \qquad (CT)$$

$$A^* + B \longrightarrow A + B^+ \qquad (Penning)$$

where A^* is an excited state that exceeds the ionization potential of B (A is often a rare gas atom).

We have already discussed the basis for the very different properties of gas-phase and solution-phase PT reactions by studies of ESPT in clusters.

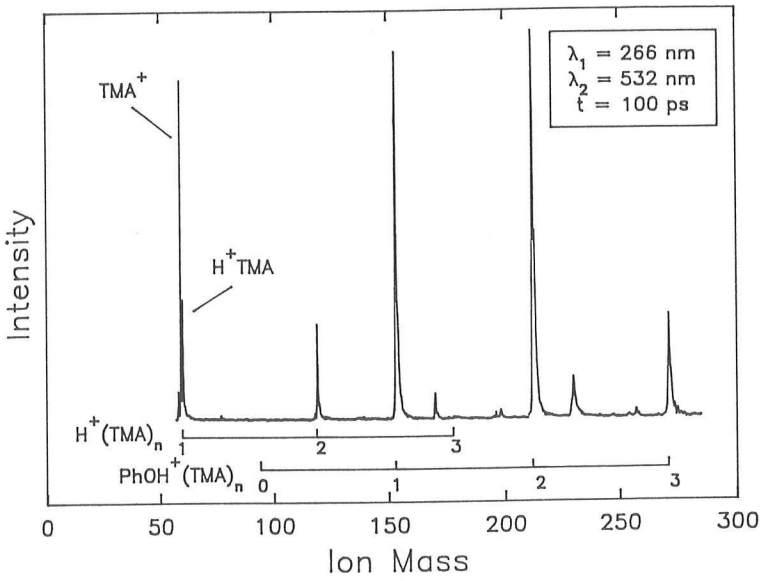

Fig. 17. Two-color picosecond TOF mass spectrum of PhOH · TMA_n clusters. An NH_3 impurity gives rise to the weak $[PhOH]^+NH_3TMA_n$ signals at 170 amu and 229 amu.

Here we present two examples of electron transfer in clusters resulting from dissociation mechanisms, namely

$$\begin{aligned} AB + h\nu &\longrightarrow A^+B \longrightarrow A + B^+ \\ CD + h\nu &\longrightarrow C^+D \longrightarrow C^+ + D \\ &\longrightarrow E + F + D^+ \end{aligned}$$

The first example occurs for ionization of phenol (A) bound to trimethylamine (B). The second example was observed for ionization and subsequent dissociative excitation of aniline (C) to C_5H_6 (E) and HNC (F) in the presence of hydrazine (D).

Phenol-trimethylamine: We have made extensive time-resolved measurements of ESPT involving PhOH with trimethylamine (TMA) cluster solvation. In accord with the higher proton affinity of TMA relative to NH_3 (9.8 vs 8.8 eV, respectively) [39], we observed a threshold solvent cluster size of $n = 3$ vs $n = 5$ for NH_3. Interesting size-dependent chemistry was also observed for the cluster ion $PhOH^+(TMA)_n$ that was not observed for $PhOH^+(NH_3)_n$. Solvent-specific chemistry is evident by comparing the mass spectra in Figure 17 (TMA solvation) with the mass spectra in Figures 12 and 13 (NH_3 solvation). The principal difference is the presence of unprotonated solvent cation (B^+) and the absence of phenol monomer cation ($PhOH^+$) for TMA solvation. The reason for this behavior is that TMA has a lower

ionization potential (7.81 eV) than the chromophore phenol (8.51 eV) [63]. Following ionization of phenol, a rapid ET occurs so that dissociation of $[PhOH \cdot TMA]^+$ leads only to $PhOH + TMA^+$, in contrast to the behavior for NH_3 solvation. When more than one TMA is bound to $PhOH^+$, the chemistry appears more like that of NH_3 solvation in that one observes signal due to H^+B_n and $[PhOH \cdot TMA_n]^+$. However, the ET has still occurred in these larger cluster ions. The solvent size-dependent chemistry for TMA is summarized as follows:

$$[PhOH \cdot TMA_n]^+ \longrightarrow \begin{cases} PhOH^+ + TMA & (X) \\ PhOH + TMA^+ & (n = 1) \\ [PhOH] \cdot TMA^+_{n-m} + TMA_m & (n > 1) \\ [PhOH] \cdot TMA_{n-m} + TMA^+_m & (X) \\ PhO + H^+TMA^+_{n-m} + TMA_m & (n > 2) \end{cases}$$

where X stands for "no reaction". The model assumes a fast electron transfer followed by one of three possible cluster-size-dependent dissociations. For $n = 1$, only one bond can break, thus producing TMA^+. The presence of TMA^+ and absence of $PhOH^+$ in Figure 17 indicates that ET is much faster than dissociation. Cluster ions for $n > 1$ preferentially dissociate a neutral TMA to preserve the stronger cluster ion-dipole bond(s). Thus, unprotonated TMA^+_n is not observed for $n > 1$ in Figure 17. For $n > 2$, ESPT is presumed to occur, leading to the formation of neutral excited state ion-pairs, which then undergo dissociative ionization to the outer-cluster ion potential well (cf. Figure 2).

These results have important implications toward understanding gas-phase and bulk-phase correspondences. In a bimolecular gas-phase collision, PhOH loses its charge to TMA. However, in clusters or the bulk phase, phenol retains proximity to charge even though it resides on a partner molecule.

Aniline-hydrazine: We undertook a study to understand how single-molecule solvation would affect the well-known ion photodissociation

$$C_6H_5NH_2^+ + h\nu \longrightarrow C_6H_5NH_2^{+*} \longrightarrow C_5H_6^+ + HNC$$

This reaction is termed metastable because of its slow rate of decay at moderately high ion energies ($k \sim 1$–$2\ \mu\ s^{-1}$ at 5–6 eV ion energy) [65]. This level of ion energy is achieved using 266-nm excitation (two-photon ionization, one-photon ion absorption) [66]. Our cluster work showed that the addition of just one or two NH_3 molecules reduces the dissociation rate by at least an order of magnitude at comparable excitation energies [7]. Yet, the reaction clearly occurs and without other competing chemistry [6].

We employed a mass-selected cluster ion dissociation technique coupled with fragment ion kinetic energy filtering to distinguish $C_5H_6^+$ formed from monomer versus solvated aniline cation [7]. However, our best evidence

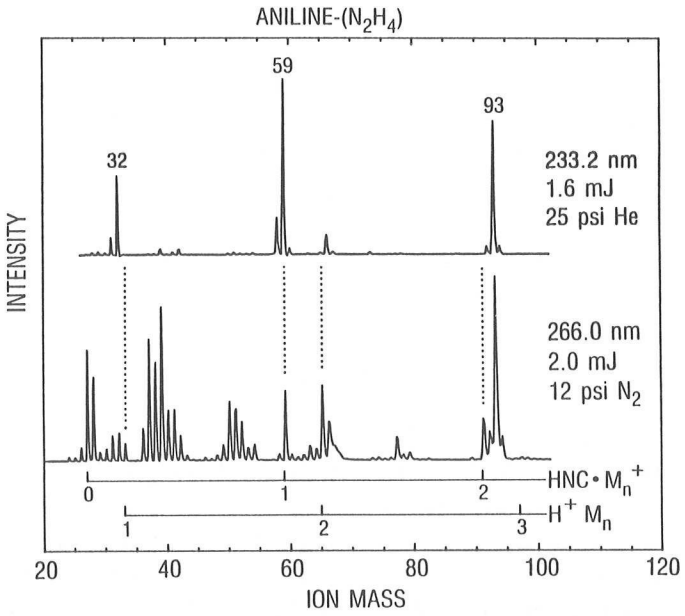

Fig. 18. Resonance ionization mass spectra of aniline-(N_2H_4) for different excitation conditions. The HNC · $(N_2H_4)_n^+$ series is evidence of a dissociation-induced electron transfer mechanism.

for solvated metastable decay was obtained inadvertently when we used hydrazine (N_2H_4) solvation [6]. We investigated a series of hydrogen bonding solvents. The solvents studied and their ionization potentials (IPs) are NH_3 (10.18 eV), N_2H_4 (8.74 eV), H_2O (12.6 eV), and CH_3OH (10.84 eV) [63]. In all cases, except N_2H_4, the mass spectra for 266-nm ionization/excitation consisted of the $C_6H_5NH_2^+ \cdot B_n$ series and $C_5H_6^+$. This result indicates that the solvent binds to the $-NH_2$ group of aniline and not the ring, as expected. However, it could not be determined whether any $C_5H_6^+$ originated from clusters.

For N_2H_4 solvation, a new reaction unfolds involving a long-range electron transfer. The mass spectra in Figure 18 reveal strong signals due to HNC · B_n^+. Solvated metastable dissociation is now evident because the otherwise neutral fragment HNC is now bound to a detectable charged molecule. The reason for the ET from N_2H_4 can be understood by considering the IP of all species involved. The chromophore aniline carries the charge in the cluster ion because of its low IP of 7.7 eV relative to that of all the solvents. Upon aniline cation dissociation, the C_5H_6 radical becomes the species with the lowest IP (8.97 vs 13.6 eV for HNC) [63] in all solvents studied except N_2H_4.

The dissociation-induced electron transfer involving N_2H_4 has several interesting implications worth noting. (1) The ET travels the length of several bonds. Also because it must occur during or after dissociation, but before a large separation takes place between fragments, the rate of ET must be very rapid. (2) The presence of HNC · B_n^+ fragments implies that the weak —NH_2 · B bond (about 1 eV bond energy) remains intact while slow and far more energetic chemistry occurs. This result would appear to violate a statistical mechanism in which energy redistribution should lead to breakage of the weakest bond. We have no explanation for this intriguing result.

5.3 PHOTOCHEMISTRY OF SULFIDE DIMER CATIONS

We have so far discussed cluster photochemistry for a variety of solute excitation conditions (bound and repulsive state excitation) and solute-solvent bonding interactions (van der Waals, hydrogen-bonding, ion-induced dipole attraction). Here we review a study of the photoexcitation of organosulfide (thioether) cluster ions formed by ionization of dimethyl sulfide (DMS) clusters [8]. These systems are unusual because the bond for the dimer ion core is "covalent" due to a three-electron, two-center interaction (3e, 2c) [67–69] represented in Figure 19a. Odd-electron bonds have a prominent role in radical chemistry, yet they are poorly understood compared with conventional two-electron neutral bonds. The three-electron sigma-like bond in the thioether dimer cation forms from the overlap of an open-shell (ion) and closed-shell (neutral) p-orbital and has a bond energy of about 25 kcal/mol ($\sim$ 1 eV) for DMS [68].

The study of reactions in cluster ions has direct correspondence to solution-phase chemistry, particularly nucleophilic displacements for which the formation of carbocations constitutes the central reactive site. Reaction intermediates for nucleophilic displacement with sulfides and halogenated sulfides often involve electropositive sulfur atoms. The stable S—S^+ bond and the alkylating nature of sulfides, which we observe in the cluster ions, are responsible for such adverse effects as the blistering action of mustard gas [2,2'–bis(chloroethyl)sulfide], or in a controlled environment are capable of beneficial effects such as the selective destruction of tumor cells in cancer treatment [70]. Sulfer-sulfer cross-linkage bonds have biochemical importance in the activity of enzymes and commercial importance in the manufacture of rubber.

The (3e, 2c) sulfide dimer cation has strong visible absorptions that are well separated from the far ultraviolet absorption of the neutral monomer and the near ultraviolet absorptions of the monomer cation [68, 69]. The origin of these blue-visible absorptions can be seen in the correlation diagram in Figure 19b. The splitting of the $3p_x$ orbitals creates a σ, σ^* transition.

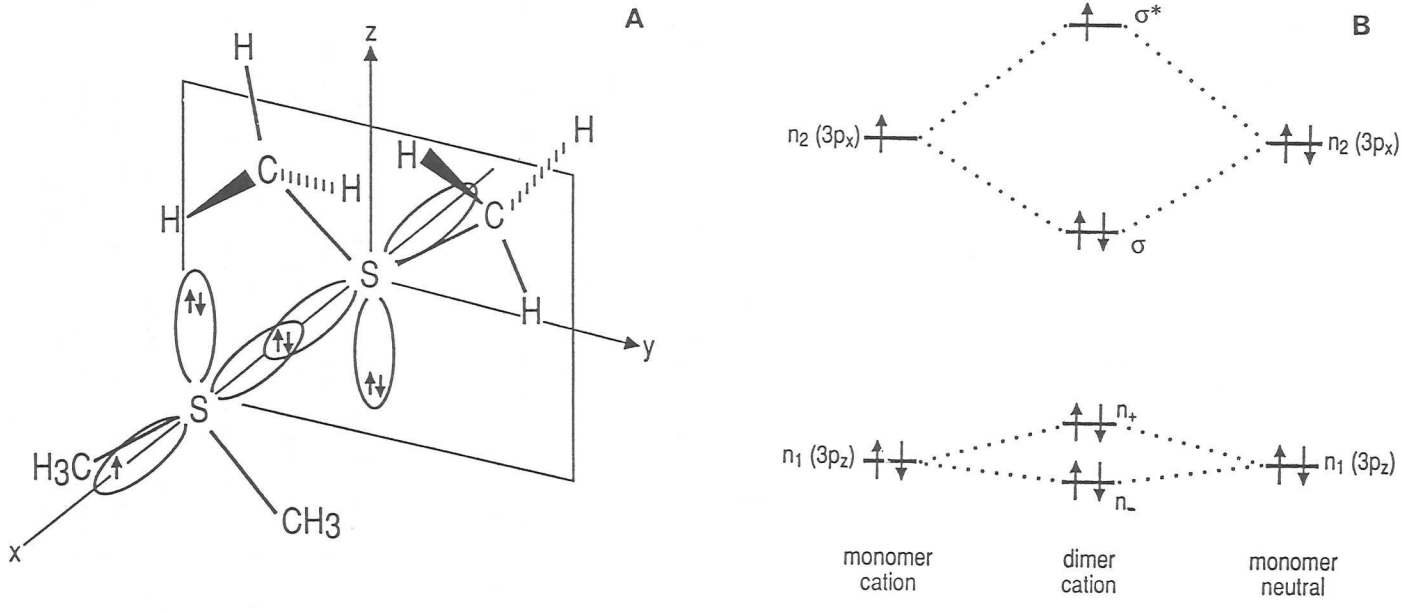

Fig. 19. (a) Geometry and coordinate system for DMS monomer and dimer cation. (b) Energy level diagram for the sulfide dimer cation. The $3p_x$ is a pure p-orbital, whereas, $3p_z$ is actually a hybrid orbital with about 25% $3s$ admixture.

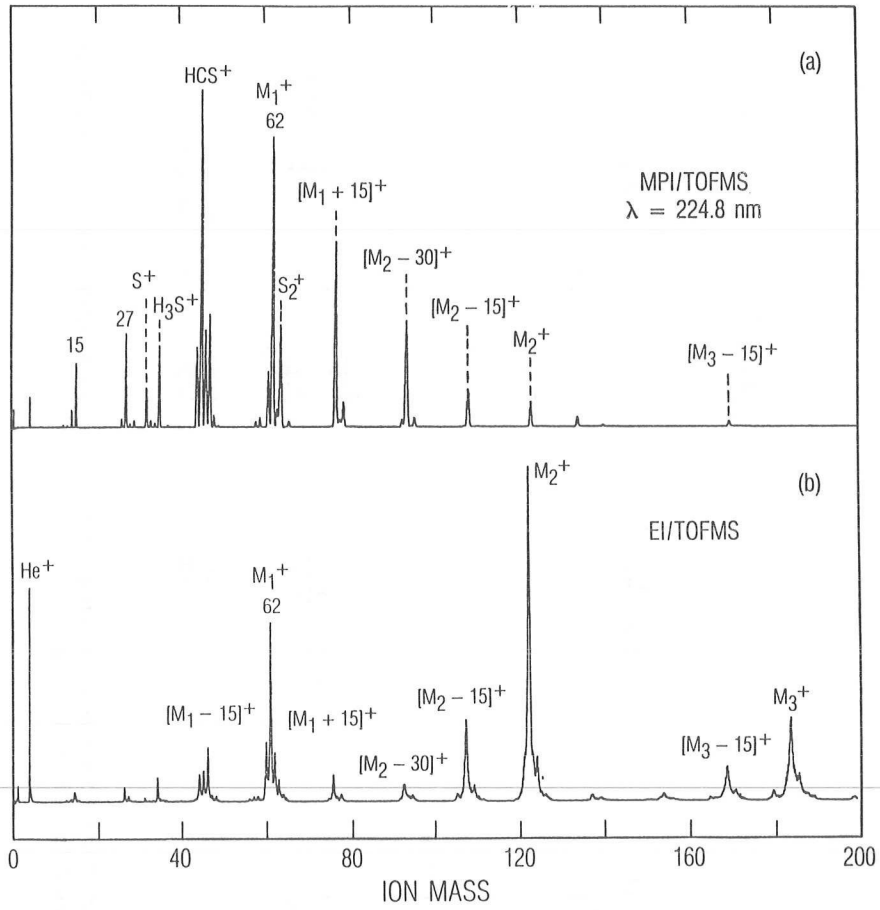

Fig. 20. Mass spectra of DMS clusters: (a) Resonance ionization and ion absorption at 225 nm. (b) EI excitation showing different fragmentation behavior.

The results in Figures 20 and 21 reveal dramatic differences in the cluster ion chemistry induced by EI and by photochemical excitation. The principal cluster ion chemistry in EI ionization/dissociation is S–C bond cleavage leading to demethylation and hydride transfer producing protonated DMS monomer and cluster ions (Figure 20b). These results are similar to what is observed in bimolecular gas-phase reactions involving DMS cation and neutral [67, 71]. Photochemical excitation, however, produces distinct photoproducts that depend strongly on wavelength. The cluster fragmentation in Figure 20a is attributable mostly to cluster ion absorption at 225-nm and leads to photoproducts S_2^+, $(CH_3)_3S^+$, CS^+, and HCS^+ that are either absent or much weaker by EI excitation.

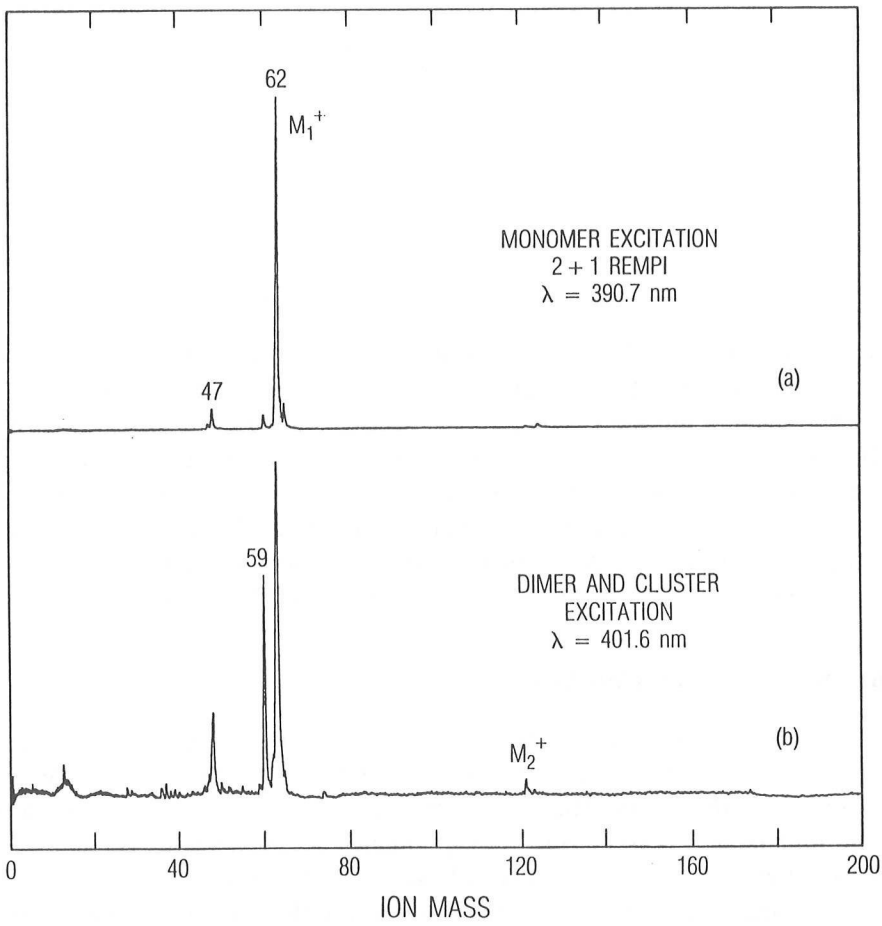

Fig. 21. Two-photon resonance, one-photon ionization mass spectra of DMS monomer and dimer/cluster: (a) monomer ionization through the origin intermediate state at 390.7 nm. (b) Dimer and cluster ionization/excitation using 401.6 nm excitation.

Cluster ion excitation to the dimer cation σ^* state at 400 nm generates entirely different chemistry than for the cases above. Cluster ions are first produced just above the ionization threshold by a two-photon resonance ($4p \leftarrow 3p_x$), one-photon ionization at wavelengths around 400 nm. Photochemistry is then promoted by subsequent ion absorption. Pulse energies were reduced so that excitation through the origin transition of DMS monomer

(51200 cm^{-1}) [72] produced little ion dissociation (Figure 21a). The excitation wavelength was shifted to the red of the monomer origin to excite primarily DMS clusters (Figure 21b). A distinctly singular peak at mass 59 was observed. The structure of mass 59 could either be an open β-thiovinyl cation or a closed cyclic thiirenium cation, namely

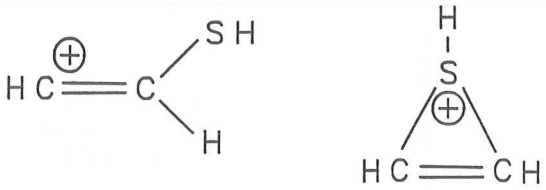

Molecular orbital calculations indicate that the cyclic form is more stable by 1–14 kcal/mol with a barrier to interconversion of about 13 kcal/mol [73].

The cyclic thiirenium structure has been postulated as a critical intermediate or transition state in certain solution-phase rearrangement and addition reactions involving organosulfide molecules [70]; however, its previous detection has been elusive. Trimethyl thiirenium has been observed by low temperature NMR [74]. Mass 59 has only been observed as a trace component in gas-phase mass spectrometry of organosulfide molecules [75].

6. Summary and Conclusions

Studies of reactivity in isolated molecular clusters are providing valuable information on the interactions of individual solvent or lattice molecules on chemical dynamics. The two main objectives of our cluster work are to gain understanding of (1) the correspondence between gas-phase and bulk-phase chemistry and (2) the dependence of chemical properties on solvent environment. Clusters are uniquely suited for these studies because their size quite naturally spans the limits of the gas phase and the bulk phase and because their specific composition and geometry are usually fairly well known. Much of our work is based on proton transfer from the molecule phenol to a hydrogen-bonding solvent cluster. This prototype system has proved valuable in addressing many of the issues above. We observed distinct cluster size thresholds for excited state proton transfer and explained the results using an energy diagram showing how the isolated gas-phase phenol excited state potentials are modified by stepwise addition of solvent molecules. Though stepwise solvent binding energies are a strong driving force to reactivity, simple additivity arguments are insufficient for describing the role of first- and second-shell solvent molecules. Mixed solvent studies with phenol showed that addition of a single dissimilar molecule to an otherwise reactive cluster can seriously suppress the rate of ESPT. We also investigated the cluster ions

as models of gas-phase reactive complexes and resolved a longstanding issue regarding double-minima potentials for ion-molecule reactions.

Our studies have yielded predictable results and surprising results. The former includes chemistry that is directly related to gas-phase or condensed-phase reactions and easily explained by simple energy arguments. The surprising results are those that are unique to the cluster environment and highlight that there is still much to be learned about chemistry in general. For example, we are baffled by how a weak solvent bond can survive an energetic reaction involving multiple breaking of much stronger bonds (aniline cation fragmention bound to N_2H_4). In another example, ionization and excitation of dimethyl sulfide clusters yielded primarily products associated with gas-phase ion molecule reactions. However, excitation of a strong dimer cation σ^* transition yielded almost exclusively the elusive cyclic thiirenium ion, implicated as a transition state immediate in a number of condensed-phase sulfide reactions.

Cluster research is a large field, but a young one. The field is still full of surprises (witness C_{60} developments). Clusters are just beginning to make serious inroads in our understanding of matter. There are broad classes of chemistry that have not yet been investigated from the perspective of clusters (photochemical rearrangements, nucleophilic displacements, stereochemistry, to name a few). Development of new research techniques involving clusters shows no sign of abating. One might expect cluster techniques to be useful for engineering nanotechnologies. Clusters are also ideally suited for studying physical properties of gas-liquid interfaces. It is certain that more application will evolve and that cluster research will remain exciting for many years to come.

Acknowledgements

I am particularly indebted to Jhobe Steadman who made large contributions to the cluster work reviewed here. These studies were supported by the Aerospace Sponsored Research program.

References

1. Bernstein, E. R., ed. *Atomic and Molecular Clusters*, (Elsevier, New York, 1990).
2. Halberstadt N. and Janda, K. C., eds.; *Dynamics of Polyatomic van der Waals Complexes*, NATO ASI Series, Vol. 227, 1990.
3. Breen, J. J., Tzeng, W.-B., Kilgore, K., Keesee, R. G., and Castleman Jr., A. W., *J. Chem. Phys.* **90**, 19 (1989); O. Echt, O., Dao, P. D., Morgan, S., and Castleman Jr., A. W., *J. Chem. Phys.* **82** 4076 (1985).
4. Garvey J. F. and Bernstein, R. B., *J. Am. Chem. Soc.* **109**, 1921 (1987); Garvey J. F. and Bernstein, R. B., *J. Phys. Chem.* **90**, 3577 (1986).

5. Bernstein, E. R., *J. Phys. Chem.* **96**, (1992).
   Brutschy, B., *J. Phys. Chem.* **94**, 8637 (1990).
6. Syage, J. A., *J. Phys. Chem.* **93**, 107 (1989).
7. Syage, J. A., *J. Chem. Phys.* **92**, 1804 (1990); Syage J. A., and Steadman, J., *Rev. Sci. Instrum.* **61**, 1204 (1990).
8. Syage, J. A., Pollard, J. E., and Cohen, R. B., *J. Phys. Chem.* **95**, 8560 (1991).
9. Mikami, N., Okabe, A., and Suzuki, I., *J. Phys. Chem.* **92**, 1858 (1988); Mikami, N., Suzuki, I., and A. Okabe, A., *J. Phys. Chem.* **91**, 5242 (1987).
10. Steadman J. and Syage, J. A., *J. Am. Chem. Soc.* **113**, 6786 (1991).
11. Syage J. A., and Steadman, J., *J. Phys. Chem.* **96**, 9606 (1992).
12. Syage J. A., and Steadman, J., *J. Chem. Phys.* **95**, 2497 (1991); Steadman J. and Syage, J. A., *J. Chem. Phys.* **92**, 1630 (1990).
13. Syage, J. A., *Chem. Phys. Lett.* **202**, 227 (1993).
14. Steadman J. and Syage, J. A., *J. Phys. Chem.* **95**, 10326 (1991).
15. Cheshnovsky, O. and Leutwyler, S., *Chem. Phys. Lett.* **121**, 1 (1985); Cheshnovsky, O. and Leutwyler, S., *J. Chem. Phys.* **88**, 4127 (1988); Droz, T., Knochenmuss, R., and Leutwyler, S., *J. Chem. Phys.* **93**, 4520 (1990).
16. Solgadi, D., Jouvet, C., and Tramer, A., *J. Phys. Chem.* **92**, 3313 (1988); Jouvet, C., Lardeux-Dedonder, C., Richard-Viard, M., Solgadi, D., and Tramer, A., *J. Phys. Chem.* **94**, 5041 (1990).
17. Breen, J. J., Peng, L. W., Willberg, D. M., Heikal, A., Cong, P., and Zewail, A. H., *J. Chem. Phys.* **92**, 805 (1990).
18. Hineman, M. F., Bruker, G. A., Kelley, D. F., and Bernstein, E. R., *J. Chem. Phys.* **97**, 3341 (1992); Kim, S. K., Li, S., and Bernstein, E. R., *J. Chem. Phys.* **95**, 3119 (1991).
19. Syage J. A. and Steadman, J., *Chem. Phys. Lett.* **166**, 159 (1990); Steadman, J., Fournier, E. W., and Syage, J. A., *Appl. Opt.* **29**, 4962 (1990).
20. Kappes M. and Leutwyler, S., in *Atomic and Molecular Beam Methods*, Vol. I, edited by G. Scoles, (Oxford University Press, New York, 1988), p. 380.
21. Syage, J. A., *Phys. Rev. A* **46**, 5666 (1992).
22. Syage, J. A., *J. Phys. B.* **24**, L527 (1991).
23. Syage, J. A., *J. Chem. Phys.* **97**, 6085 (1992).
24. Syage, J. A., Pollard, J. E., and Steadman, J., *Chem. Phys. Lett.* **161**, 103 (1989).
25. Syage J. A. and Steadman, J., *J. Chem. Phys.* manuscript in preparation.
26. Trevor, D. J., Van Woerkom, L. D., and Freeman, R. R., *Rev. Sci. Instrum.* **60**, 1051 (1989); Liu, G., Barton, J. J., Bahr, C. C., and Shirley, D. A., *Nucl. Instr. and Meth.*, **A246**, 504 (1986).
27. Steadman J. and Syage, J. A., *Rev. Sci. Instrum.*, in press.
28. Ray, D., Levinger, N. E., Papanikolas, J. M., and Lineberger, W. C., *J. Chem. Phys.* **91**, 6533 (1989); Papanikolas, J. M., Gord, J. R., Levinger, N. E., Ray, D., Vorsa, V., and Lineberger, W. C., *J. Phys. Chem.* **95**, 8028 (1991).
29. Kazishka, A. J., Shchuka, M. I., Wittmeyer, A. S., and Topp, M. R., *J. Phys. Chem.* **95**, 3663 (1991).
30. Felker P. M. and Zewail, A. H., *Chem. Phys. Lett.* **94**, 448, 454 (1983); Connell, L. L., Ohline, S. M., Joireman, P. W., Corcoran, T. C., and Felker, P. M., *J. Chem. Phys.* **96**, 2585 (1992).
31. Cassasa, M. P., Stephenson, J. C., and King, D. S., *J. Chem. Phys.* **89**, 1966 (1988).
32. Sipior J. and Sulkes, M., *J. Chem. Phys.* **88**, 6146 (1988); Teh, C. K., Sipior, J., and Sulkes, M., *J. Phys. Chem.* **93**, 5393 (1989); Arnold S. and Sulkes, M., *J. Phys. Chem.* **96**, 4768 (1992).
33. Fuke, K., Keizo, K., Misaizu, F., and Kaya, K., *J. Chem. Phys.* **95**, 4074 (1991).
34. Woodward, A. M., Colson, S. D., Chupka, W. A., and White, M. G., *J. Phys. Chem.* **90**, 274 (1986); Walter, K., Weinkauf, R., Boesl, U., and Schlag, E. W., *J. Chem. Phys.* **89**, 1914 (1988).
35. Kosower E. M., and Huppert, D., *Annu. Rev. Phys. Chem.* **37**, 127 (1986).

36. Lee, J., Griffin, R. D., and Robinson, G. W., *J. Chem. Phys.* **82**, 4920 (1985); Lee, J., Robinson, G. W., Webb, S. P., Philips, L. A., and Clark, J. H., *J. Am. Chem. Soc.* **108**, 6538 (1986)
37. Huppert, D. H., Jayaraman, A., Maines Sr., R. G., Steyert, D. W., and Rentzepis, P. M., *J. Chem. Phys.* **81**, 5596 (1984).
38. Gonohe, N., Abe, H., Mikami, N., and Ito, M., *J. Phys. Chem.* **89**, 3642 (1985); Oikawa, A., Abe, H., Mikami, N., and Ito, M., *J. Phys. Chem.* **87**, 5083 (1983).
39. Lias, S. G., Liebman, J. F., and Levin, R. D., *J. Phys. Chem. Ref. Data* **13**, 695 (1984).
40. Kebarle, P., *Annu. Rev. Phys. Chem.* **28**, 445 (1977); Grimsrud E. P. and Kebarle, P., *J. Am. Chem. Soc.* **95**, 7939 (1973); Mautner M. J. and Speller, C. V., *J. Phys. Chem.* **90**, 6616 (1986).
41. Ireland J. F. and Wyatt, P. A. H., *Adv. Phys. Org. Chem.* **12**, 131 (1976).
42. Price, J. M., Crofton, M. W., and Lee, Y. T., *J. Phys. Chem.* **95**, 2182 (1991).
43. Pimentel G. C. and McClellan, A. L., *The Hydrogen Bond*, (W. H. Freeman, San Francisco, 1960); Dykstra, C. E., *J. Phys. Chem.* **94**, 6948 (1990).
44. Peteanu L. A. and Levy, D. H., *J. Phys. Chem.* **92**, 6554 (1988); Champagne, B. B., Pfanstiel, J. F., Plusquellic, D. F., Pratt, D. W., van Herpen, W. M., and Meerts, W. L., *J. Phys. Chem.* **94**, 6 (1990).
45. Venturo, V. A., Maxton, P. M., and Felker, P. M., *J. Phys. Chem.* **96**, 5234 (1992); Connell, L. L., Corcoran, T. C., Joireman, P. W., and Felker, P. M., *J. Phys. Chem.* **94**, 1229 (1990).
46. Wessel J. E. and Syage, J. A., *J. Phys. Chem.* **94**, 737 (1990); Syage J. A. and Wessel, J. E., *J. Chem. Phys.* **89**, 5962 (1988).
47. Wei, S., Shi, Z., and Castleman Jr. A. W., *J. Chem. Phys.* **94**, 3268 (1991).
48. Maroncelli, M., MacInnis, J., and Fleming, G. R., *Science* **243**, 1674 (1989); Rothenberger, G., Negus, D. K., and Hochstrasser, R. M., *J. Chem. Phys.* **79**, 5360 (1983).
49. Simon, J. D., *Acc. Chem. Res.* **21**, 128 (1988); Su S.-G. and Simon, J. D., *J. Chem. Phys.* **89**, 908 (1988).
50. Barbara, P. F., Walker, G. C., and Smith, T. P., *Science,* **256**, 975 (1992); Jarzeba, W., Walker, G. C., Johnson, A. E., Kahlow, M. A., and Barbara, P. F., *J. Phys. Chem.* **92**, 7039 (1988); Kozik, M., Sutin, N., and Winkler, J. R., *Coord. Chem. Rev.* **97**, 23 (1990).
51. Anderson, J. G., Toohey, D. W., and Brune, W. H., *Science* **251**, 39 (1991).
52. Schwartz S. E., and White, W. H., in *Trace Atmospheric Constituents: Properties, Transformations, and Fates*, (John Wiley and Sons, New York, 1983).
53. Knee, J. L., Khundkar, L. R., and Zewail, A. H., *J. Chem. Phys.* **83** 1996 (1985).
54. Sapers, S. P., Vaida, V., and Naaman, R., *J. Chem. Phys.* **88** 3638 (1988).
55. Wang, P. G., Zhang, Y. P., Ruggles, C. J., and Ziegler, L. D., *J. Chem. Phys.* **92**, 2806 (1990).
56. Fan and Y. B., Donaldson, D. J., *J. Phys. Chem.* **96**, 19 (1992).
57. Sparks, R. K., Shobatake, K., Carlson, L. R., and Lee, Y. T., *J. Chem. Phys.* **75** 3838 (1981).
58. Wittig, C., Sharpe, S., and Beaudet, R. A., *Acc. Chem. Res.* **21**, 341 (1988); Radhakrishnan, G., Buelow, S., and Wittig, C., *J. Chem. Phys.* **84**, 727 (1986).
59. Halberstadt N. and Soep, B., *J. Chem. Phys.* **80**, 2340 (1984).
60. Moylan C. R. and Brauman, J. I., *Annu. Rev. Phys. Chem.* **34**, 187 (1983); (b) Comita P. B. and Brauman, J. I., *Science* **227**, 863 (1985); Bowers, M. T., ed. *Gas Phase Ion Chemistry*, Vols. I and II, (Academic Press, New York, 1979).
61. Farneth W. E. and Brauman, J. I., *J. Am. Chem. Soc.* **98**, 7891 (1976); Jasinski J. M. and Brauman, J. I., *J. Am. Chem. Soc.* **102**, 2906 (1980).
62. Cyr, D. M., Bishea, G. A., Scarton, M. G., and Johnson, M. A., *J. Chem. Phys.* **97**, 5911 (1992).
    Cyr, D. M., Posey, L. A., Bishea, G. A., Han, C.-C., and Johnson, M. A., *J. Am. Chem. Soc.* **113**, 9697 (1991).
63. Lias, S. G., Bartmess, J. E., Liebman, J. F., Holmes, J. L., Levin, R. D., and Mallard, W. G., *J. Phys. Chem. Ref. Data* **17**, 1 (1988).

64. Lowry T. H. and Richardson, K. S., *Mechanism and Theory in Organic Chemistry*, (Harper and Row, New York, 1976).
65. Baer T. and Carney, T. E., *J. Chem. Phys.* **76**, 1304 (1982).
66. Proch, D., Rider, D. M., and Zare, R. N., *Chem. Phys. Lett.* **81**, 430 (1981); Kühlewind, H., Neusser, H. J., and Schlag, E. W., *J. Chem. Phys.* **82**, 5452 (1985).
67. Clark, T., *J. Am. Chem. Soc.* **110**, 1672 (1988); Illies, A. J., Livant, P., and McKee, M. L., *J. Am. Chem. Soc.* **110**, 7980 (1988).
68. Asmus, K.-D., *Acct. Chem. Res.* **12**, 436 (1979).
69. Naito, A., Akasaka, K., and Hatano, H., *Mol. Phys.* **44**, 427 (1981).
70. Block, E., *Reactions of Organosulfur Compounds*, (Academic Press, New York, 1978), Chap. 4.
71. Drewello, T., Lebrilla, C. B., Schwarz, H., de Koning, L. J., Fokkens, R. H., Nibbering, N. M. M., Anklam, E., and Asmus, K.-D., *J. Chem. Soc. Chem. Commun.*, 1381 (1987); Musker, W. K., Gorewit, B. V., Roush, P. B., and Wolford, T. L., *J. Org. Chem.* **43**, 3235 (1978).
72. Syage, J. A., Pollard, J. E., and Cohen, R. B., *Appl. Opt.* **26**, 3516 (1987).
73. Csizmadia, I. G., Duke, A. J., Lucchini, V., and Modena, G., *J. Chem. Soc. Perkin Trans. II*, 1808 (1974).
74. Capozzi, G., DeLucchi, O., Lucchini, V., and Modena, G., *Chem. Commun.*, 248 (1975).
75. Möckel, H. J., *Fresenius Z. Anal. Chem.* **295**, 241 (1979).

(1) It is possible to measure properties of individual cluster sizes by optically-selective excitation and mass-resolved detection. A series of measurements as a function of cluster size provides direct information on how properties such as reactivity, electronic-state energies, energy and structural relaxation, etc. are influenced by addition of single molecules. (2) Because the internal energy of the clusters can be made low relative to the photoexcitation energy, the excited-state clusters are essentially isoenergetic and constitute a microcanonical ensemble (i.e., an ensemble of noninteracting subsystems at constant energy). Thermal averaging effects are minimized in photochemical cluster studies. (3) The specific cluster size, composition (e.g., when using mixed solvents), and geometry are often known making it possible to explore specific structural and solvent-core effects that would otherwise be averaged out in condensed-phase studies.

In this article, we review some of our recent work in cluster chemistry. Many of the examples we show can be classified as well-behaved cluster chemistry. These are cases where the observed chemistry corresponds to known reactions in the gas phase or condensed phase and is readily explanable by simple thermochemical models. More interesting are the unusual and unexpected results that can be attributed to some specific cluster environment such as structure and composition of an inner solvent shell. These effects would be obscured in condensed-phase studies, which measure an averaged solvent environment. From cluster work emerges a deeper understanding of the role of solvation and structure on chemical reactivity. We will cover two themes. (1) Chemical reactivity, as measured by rate of reaction, is investigated for specific solvent compositions and size. These studies include the use of mixed solvents to examine impurity effects. Time-resolved methods for measuring dynamics of solvent reorganization (i.e., "solvation") will also be discussed. (2) The correspondence between gas-phase to condensed-phase chemistry is investigated as a function of cluster size. These include studies to observe the onset to condensed-phase chemistry with increasing cluster size as well as studies to show both gas-phase and condensed-phase type chemistry in clusters that occur in relative proportions that are strongly dependent on the excitation process.

2. Experimental Methods

Most of our work employs multiphoton ionization and mass spectrometry. We have recently brought on line a time-of-flight photoelectron spectrometer of unusual design and a free jet chamber employing ellipsoidal reflection optics for detecting laser induced fluorescence. We describe these systems below:

(1) The molecular beam time-of-flight (TOF) mass spectrometer (MS) system pictured in Figure 1a is our work-horse apparatus. It employs a

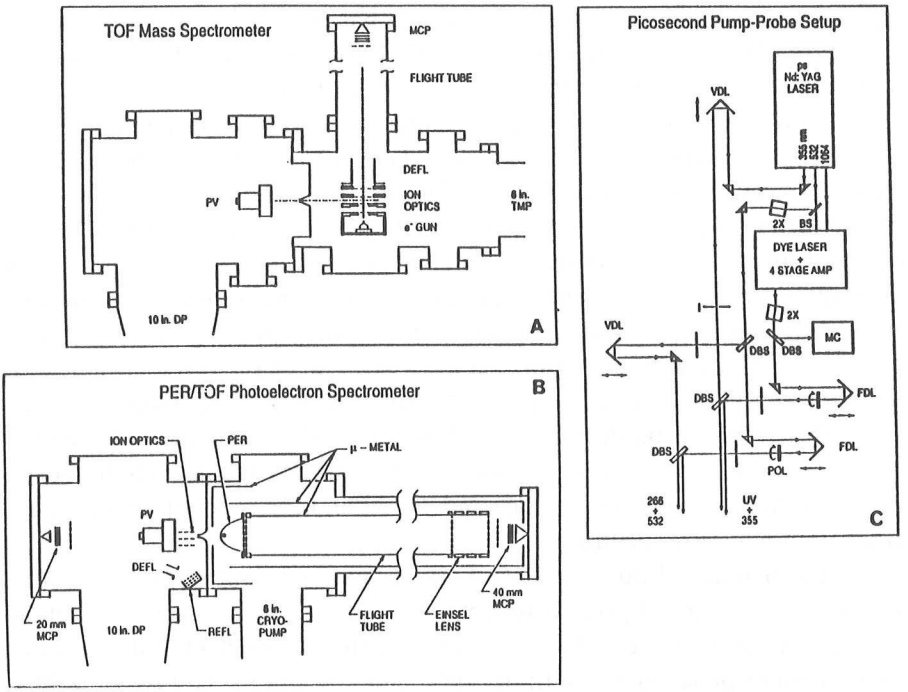

Fig. 1. Experimental schematic: (a) Molecular beam mass spectrometer, (b) molecular beam photoelectron spectrometer, (c) picosecond pump-probe arrangement. Terms are defined as follows: BS – beam splitter; DBS – dichroic beam splitter; DEFL – deflector plates; DP – diffusion pump; FDL – fixed delay line; I – iris; MC – monochromator; MCP – microchannel plate detector; PER – paraboloidal electrostatic reflector; POL – polarization rotator, PV – pulsed valve; REFL – reflecting grids; TMP – turbomolecular pump; VDL – variable delay line, 2X – doubling crystal period.

temperature-controlled pulsed valve that can be remotely positioned along three-axes during experiments. The free-jet expansion is skimmed and the resulting collimated beam is passed through a set of TOF ion optics. Three types of experiments are conducted in this apparatus. Multiphoton ionization is used for time-resolved measurements by picosecond pump-probe excitation [11–14, 19] and for spectroscopic measurements by nanosecond excitation. Electron-impact (EI) ionization is used to measure ionization cross sections in non-cluster experiments [21–23], to monitor cluster distributions as a function of pulsed valve conditions, and to measure thermochemical thresholds for cluster ion fragments. Finally, a combination of EI ionization, mass filtering, and laser photodissociation is used to measure size-specific electronic spectra and fragmentation mechanisms of cluster ions [7, 24, 25].

(2) Molecular beam photoelectron spectroscopy (PES) is carried out in an apparatus shown in Figure 1b. This device is based on a new concept of using a paraboloidal electrostatic reflector (PER) [26] to dramatically increase the collection efficiency of electrons detected by TOF energy analyzers [11, 13, 27]. This feature is crucial for studies using low energy laser pulses (e.g., in ultrafast spectroscopy) and for clusters where the density for any particular cluster size in the molecular beam can be very low. The chamber containing the pulsed valve also includes ion acceleration optics and a reflectron device for recording ion mass spectra. Because PES does not distinguish electrons originating from different cluster masses it is important to choose systems that have well characterized cluster spectroscopy so that specific cluster sizes can be selected by optical excitation. Alternatively, we have some capacity for detecting mass-selective PES spectra by simultaneously recording ion mass spectra (chamber I) and PES spectra (chamber II). Pulsed valve and excitation conditions can be adjusted to enhance or discriminate against certain cluster sizes and these changes in the mass spectrum can be correlated with changes in the photoelectron spectrum.

(3) Laser induced fluorescence of cluster products is detected in another apparatus using an ellipsoidal reflector to collect a large fraction of emission. Emission is dispersed in a monochromator and detected using a fast microchannel plate photomultiplier tube and a scanning 100-ps wide boxcar gate. Future experiments will include time-resolved stimulated emission pumping and fluorescence depletion measurements to monitor the progress of cluster dynamics in excited electronic states.

In order to sort out the variety of cluster processes that can occur simultaneously, it is necessary to employ a battery of excitation and interrogation techniques. The ones we most commonly use are described below:

(1) Picosecond pump-probe is used to initiate (pump) excited neutral reactions and detect (probe) by delayed ionization. A number of possible choices for the pump and probe pulses are available from the Nd:YAG harmonics and the dye laser (the latter employs the usual wavelength extension capabilities, e.g., doubling, mixing, Raman shifting). Two readily available and frequently used pump-probe arrangements are shown in Figure 1c. One arrangement uses the Nd:YAG harmonics, 266 nm as the pump and 532 nm (or 355 nm) as the probe. The other arrangment uses tunable UV output from the dye laser as the pump and 355 nm as the probe. We employ other combinations on occasion for both cluster and non-cluster work (i.e., 266 + Vis, UV + 532, UV + Vis). The number of labs besides our own combining time-resolved methods and cluster studies is small, but growing steadily [17, 18, 28–33].

(2) Nanosecond excitation and ionization is used to study cluster-ion properties [6–8, 11]. In some cases, the cluster ions are photoexcited to initiate chemistry [7, 8]. The cluster ion energies can be controlled to some extent

by controlling laser intensity and wavelength and choosing appropriate intermediate molecular excited states for the resonance ionization. Two-color arrangements are used to resonantly threshold ionize or to ionize and then resonantly photodissociate the ions.

(3) Electron-impact (EI) ionization is used for several purposes. We use low-energy EI to record cluster mass spectra as a diagnostic for adjusting our cluster source conditions to produce some desired cluster distribution. Another fruitful use of EI is as a convenient and non-selective ionization source for cluster-ion photodissociation studies. The method was particularly useful for our work on $(CH_3I)_n^+$ photodissociation spectra and dissociation mechanisms [7, 24, 25]. It is difficult to form $(CH_3I)_n^+$ parent ions by laser excitation because the first excited state is dissociative, which competes with ionization, and because the higher excited bound states require two-photon excitations at pulse energies that typically fragment the cluster ions [34].

The cluster samples were prepared by a variety of procedures. Solid compounds, such as phenol and aniline, were placed in a sample holder in the pulsed valve and heated to 40–60°C. For ammonia solvation, a 2-liter high-pressure cylinder was made up containing 1–10% ammonia in helium or argon. Water and methanol solvation was achieved by flowing helium through a bubbler containing either of these solvents. The CH_3I samples were prepared by flowing Ar (20–30 psia) through a bubbler that was cooled in a bath of dry ice/acetone or ice water, depending on the extent of clustering desired.

3. Excited State Proton Transfer

Aromatic alcohols are known to be more acidic in their S_1 state than in S_0 (i.e., the so-called pH jump) [35]. These reactions have been studied extensively in the condensed phase including several time-resolved experiments [35–37]. Cheshnovsky and Leutwyler pioneered the study of excited-state proton transfer (ESPT) in clusters by studying the system 1-naphthol-$(NH_3)_n$ [15]. The steady-state mass spectra and emission spectra they recorded using nanosecond excitation indicated a cluster size threshold for reaction of $n = 4$. Solgadi *et al.* measured steady-state threshold ionization curves for phenol-$(NH_3)_n$ and also reported an ESPT threshold of $n = 4$ [16], even though phenol is believed to be a weaker acid than naphthol. We have carried out mass-resolved picosecond measurements of the phenol (PhOH) ESPT reaction. The proton transfer, represented by

$$\mathrm{PhOH}^* \cdot \mathrm{B}_n \underset{k}{\longrightarrow} \mathrm{PhO}^{*-}\mathrm{H}^+\mathrm{B}_n$$

corresponds to a conversion from the locally excited S_1 state of the phenol acid to an excited ion-pair state (B_n refers to the solvent cluster consisting

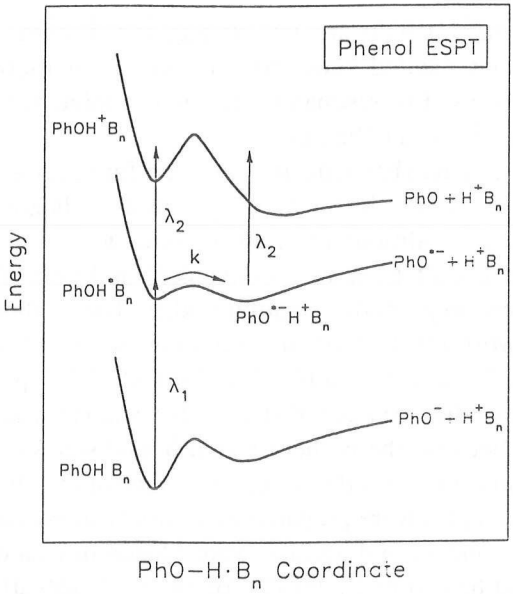

Fig. 2. Energy diagram for PhOH · $(NH_3)_n$ consistent with a cluster size of $n \sim 5$. ESPT produces an excited state ion-pair product that is ionized to the weakly-bound outer potential well of the cluster ion.

of n molecules of base B). Approximate potential energy curves for the relevant ground, excited, and ionic states of the cluster are shown in Figure 2 along with the picosecond pump-probe excitation/detection scheme used to measure the chemical rates. The energy curves are strongly dependent on solvent cluster size and basicity (explained below). The illustration given in Figure 2 approximates the case for phenol-$(NH_3)_5$. Reactant and product are distinguishable by mass spectrometry because each species fragments differently upon ionization (Figure 2). Ionization of reactant clusters PhOH* $\cdots$ B_n produces the cluster ions $PhOH^+ \cdots B_n$ on the inner potential well that are strongly bound along the O—H coordinate. Whereas, ionization of the product ion-pairs $PhO^{*-} \cdots H^+B_n$ produces cluster ions PhO$\cdots H^+B_n$ on the outer well that dissociate readily to give H^+B_n. These ion signals are convenient probes of the dynamics along the neutral excited S_1/ion-pair reactive surface.

3.1 Stepwise Solvation Properties

Phenol, in a variety of solvent clusters, was excited at 266 nm. The excess energies for NH_3 solvation range from about 1900 cm^{-1} ($n = 1$) to about 2250–2800 cm^{-1} (estimated for $n = 3-7$) [16, 38]. The S_1 origin of uncomplexed phenol is at 274.7 nm [38]. A set of reactant decay measurements are presented in Figure 3 (λ_2 = 532 nm) as a function of solvent cluster

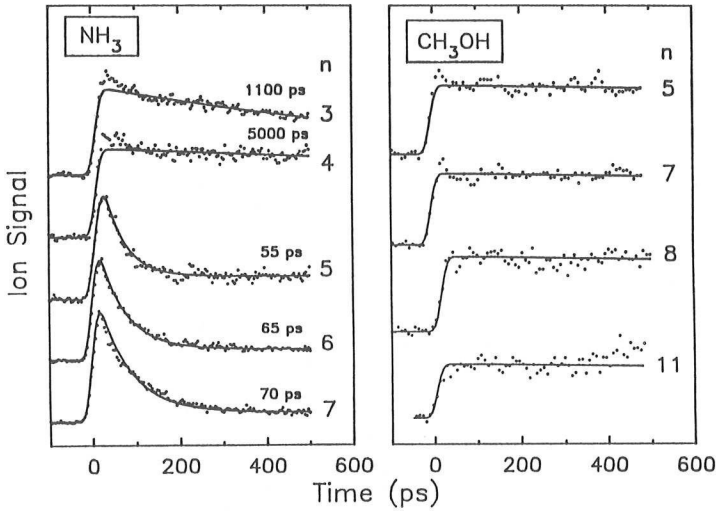

Fig. 3. Observed lifetime of the reactant $PhOH^* \cdot B_n$ (as measured by $PhOH^+ \cdot B_n$ detection) in solvent clusters $(NH_3)_n$ and $(CH_3OH)_n$. The calculated curves are described in [12]. Calculated curves for the $(CH_3OH)_n$ data assume a 10 ns lifetime.

size n for the solvents NH_3 and CH_3OH. A distinct threshold for ESPT was observed for NH_3 solvation at $n = 5$. However, no reaction was observed for CH_3OH solvation (up to $n = 11$, Figure 3). Results for other solvents are given elsewhere [12].

The reaction threshold observed for $(NH_3)_n$ solvation at $n = 5$ is due largely to stabilization of the ion-pair Coulombic potential by the proton affinity of NH_3. The ion-pair or proton-transfer states in clusters (or condensed phase) correspond to gas-phase charge transfer states. These gas-phase states, shown in Figure 4a, occur at very high energy relative to the covalent S_1 state because of the large energy required to form a free proton (the H atom ionization potential is 13.6 eV). States with large proton character, however, are stabilized enormously by complexation to molecules with high proton affinity. The interaction of a single NH_3 to PhOH is shown in Figure 4b to reduce the energy of the charge-transfer or ion-pair state dramatically relative to S_1. (NH_3 has a proton affinity of 8.8 eV) [39]. The stabilization energy for successive NH_3 molecules becomes less and less (the stepwise proton affinity) [40], however, the cumulative stabilization can be enough to lower the energy of the ion-pair state to below that of the S_1 state, thus making ESPT thermodynamically allowed. The experimental measurements indicate that this occurs for five NH_3 molecules and the calculated potentials in Figure 4c are in near agreement with this result.

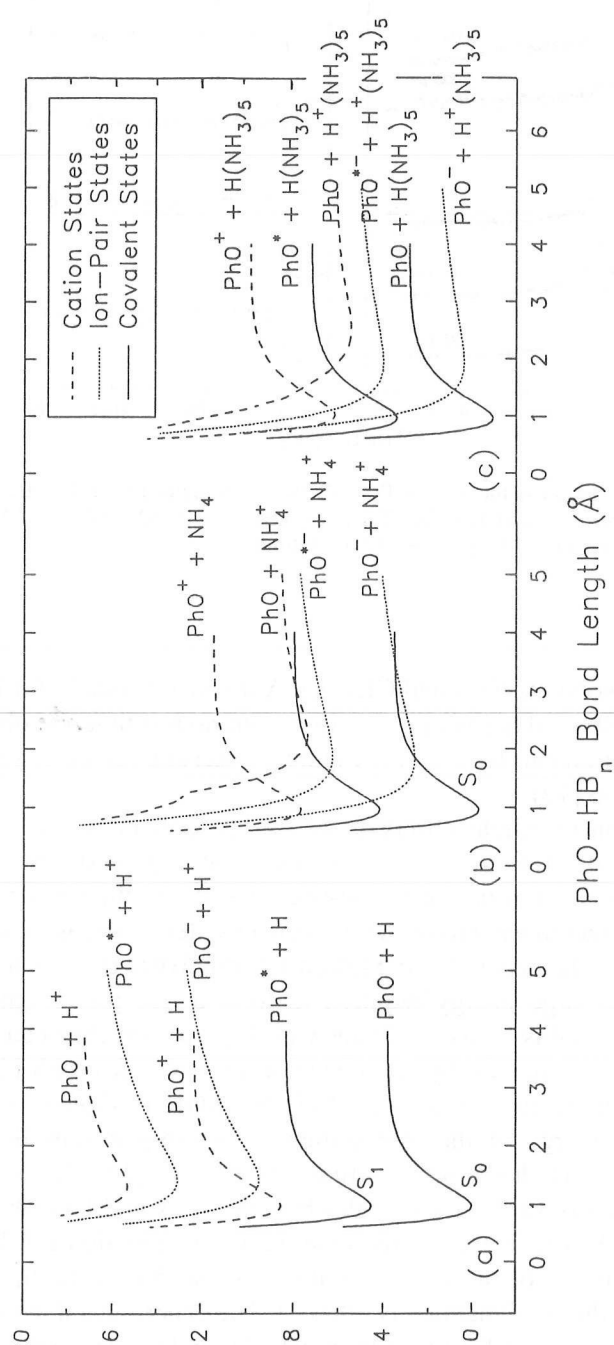

Fig. 4. Approximate PhOH · $(NH_3)_n$ cluster potential energy curves for the reactive PhO—H coordinate. (a) $n = 0$, (b) $n = 1$, and (c) $n = 5$.

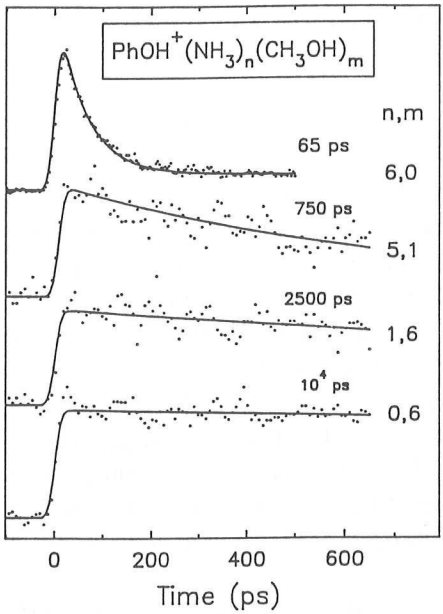

Fig. 5. Measured rates of ESPT for the mixed solvent clusters $PhOH^*(NH_3)_n(CH_3OH)_m$ using 266-nm pump and 532-nm probe excitation.

If the rates of ESPT in Figure 3a are plotted versus n, the resulting curve takes on a shape and inflection that is reminiscent of an acid-base titration curve. The similarity arises because our mass-specific, time-resolved cluster experiments are, in fact, a *single molecule titration* measurement. In similar experiments by Zewail and coworkers [17], and Bernstein, Kelley, and coworkers [18] on 1-naphthol-$(NH_3)_n$, a threshold solvent cluster size of $n = 3$ was observed for ESPT versus $n = 5$ for phenol. This is consistent with the more acidic 1-naphthol molecule [41] requiring fewer base molecules to dissociate the proton.

3.2 Disruption of the Solvent Structure

Adding a dissimilar solvent molecule to an otherwise pure solvent cluster can cause a change in the hydrogen bonding network that can disrupt proton transfer. Reaction rates for mixed solvent distributions $PhOH \cdot (NH_3)_n(CH_3OH)_m$ of similar cluster size ($n + m = 6$ or 7) were measured and are presented in Figure 5. The substitution of a single CH_3OH molecule for an NH_3 molecule causes a substantial decrease in reaction rate. Excited phenol in neat NH_3 solvent cluster $(n, m) = (6, 0)$ reacts in 65 ps whereas the $(5, 1)$ cluster reacts in 750 ps. Because the (5,0) cluster reacts in 60 ps (Figure 3), the (5,1) result indicates that the mere *addition* of a CH_3OH molecule effectively "poisons"

the reactivity of the (5,0) cluster. This is quite surprising because one would not expect the proton affinity of the solvent to decrease by simply adding CH_3OH.

An explanation for the slowed reaction is that CH_3OH acts as an intruder that disrupts the hydrogen bonding network of the neat $(NH_3)_n$ solvent structure that is crucial to solvating and stabilizing the dissociated proton [36, 37]. It is known from gas-phase cluster studies that the closed-shell structure $NH_4^+(NH_3)_4$ is very favorable for stabilizing a proton [40, 42]. However, spectroscopic and mass spectrometric evidence for the mixed NH_3/CH_3OH solvation of PhOH indicates that NH_3 forms the stronger bond to PhOH, but that CH_3OH forms the stronger bond to PhOH · NH_3 [14]. The experimental evidence is supported by reports that the NH_3—CH_3OH bond is stronger than the NH_3—NH_3 bond [43]. Consequently, given a chance, CH_3OH will displace NH_3 from the first solvation shell and prevent a pure NH_3 solvent cluster from forming. Also CH_3OH can form a stable hydrogen bond to the phenol oxygen which diminishes excited state acidity, whereas NH_3 avoids that site [38].

The concept of critical solvent structures in ESPT reactions has been investigated in the solution phase by Robinson and coworkers [36]. Their picosecond measurements and theoretical analyses on aromatic acids (e.g., 1- and 2-naphthol) in H_2O and alcohol (CH_3OH and C_2H_5OH) support the notion that a critical solvent cluster core is necessary to act as an efficient proton acceptor. For 2-naphthol in H_2O, the critical solvent-core size is about four [36].

Although, the structure of clusters that involve hydrogen bonds can often be deduced or determined from optical shifts and mass spectral distributions, direct spectroscopic measurement of solvent structure about a reactive solute molecule has not yet been made. Advances in high resolution spectroscopy [44–46] and new applications in mass spectrometry [14, 47] are beginning to yield information on the bonding structure of homogeneous and mixed clusters; however, these efforts are young. Progress in understanding the influence of solvent structure on chemical reactivity and other dynamical processes will benefit greatly by a closer association of dynamicists and spectroscopists.

3.3 Solvent Reorganization in Clusters

As a consequence of proton transfer, the solvent is no longer at equilibrium because of the large dipole formed by the charge separation along the O—H coordinate. This is a substantial perturbation that should give rise to further

dynamics in the cluster. We represent the separation of reaction and solvent dynamics as

$$PhOH^* \cdots B_n \underset{k}{\longrightarrow} [PhO^{*-} \cdots H^+B_n]_{ur} \underset{k_s}{\longrightarrow} [PhO^{*-} \cdots H^+B_n]_r$$

where the subscripts ur and r denote unrelaxed and relaxed solvent configurations and k_s is the solvent relaxation rate constant. The product formation curves in Figure 6a show two time-dependences, a rapid rise that matches the decay of the $PhOH^+ \cdot (NH_3)_n$ signals (55–70 ps) and a much slower growth component of about 300 ps. The fast time response is due to the ESPT reaction. The slow time response is ascribed to solvent cluster reorganization.

How the potential energy along the O—H coordinate might change with time due to solvent reorganization is illustrated qualitatively in Figure 6b. The solvent network must reorganize to achieve a structure that best accomodates the proton. This reorganization or "solvation of the proton" causes delocalization of charge and lengthening of the O—H bond. The relaxing ion-pair moves closer to a geometry representing the cluster-ion equilibrium configuration. This improves the Franck-Condon (FC) factors for ionization and leads to an increased ionization efficiency with time. The curves in Figure 6c were calculated for different relative ionization efficiencies from the unrelaxed (i_b) and relaxed (i_c) product clusters. The details of this simple kinetic model are given elsewhere [12]. The calculations that best fit the data in Figure 6a are indeed those for which the ionization efficiency increases with time. These results are consistent with Franck-Condon factors for ionization that improve as a result of solvent reorganization.

A more definitive measure of geometry change is to monitor individual FC components to ionization [13]. This is achieved by time-resolved photoelectron spectroscopy. Figure 7 contains photoelectron spectra (PES) for different probe delay times. The spectra are broad because of the distribution of cluster sizes, large density of low frequency modes, rapid vibrational redistribution, and large geometry change upon ionization. The $t = -100$ ps spectrum is identical to the 266 nm only spectrum (not shown) and therefore corresponds to ionization to the $PhOH^+ \cdot (NH_3)_n$ complex (Figure 2 or 7b). For positive t a low electron energy band appears. Low-energy electrons correspond to high-energy ions and would be the outcome of poor FC factors to ionization. However, in time, the solvent reorganizes to better solvate the proton and evolves to a geometry that is more similar to the ion geometry. Consequently, the FC factors for ionization improve (become more vertical), thus producing lower energy ions (i.e., higher energy electrons). Hence, the PES is expected to shift from low electron energy to high electron energy. This effect is analogous to that which causes the time dependence of emission bands used to measure solvent relaxation in the condensed phase [48–50].

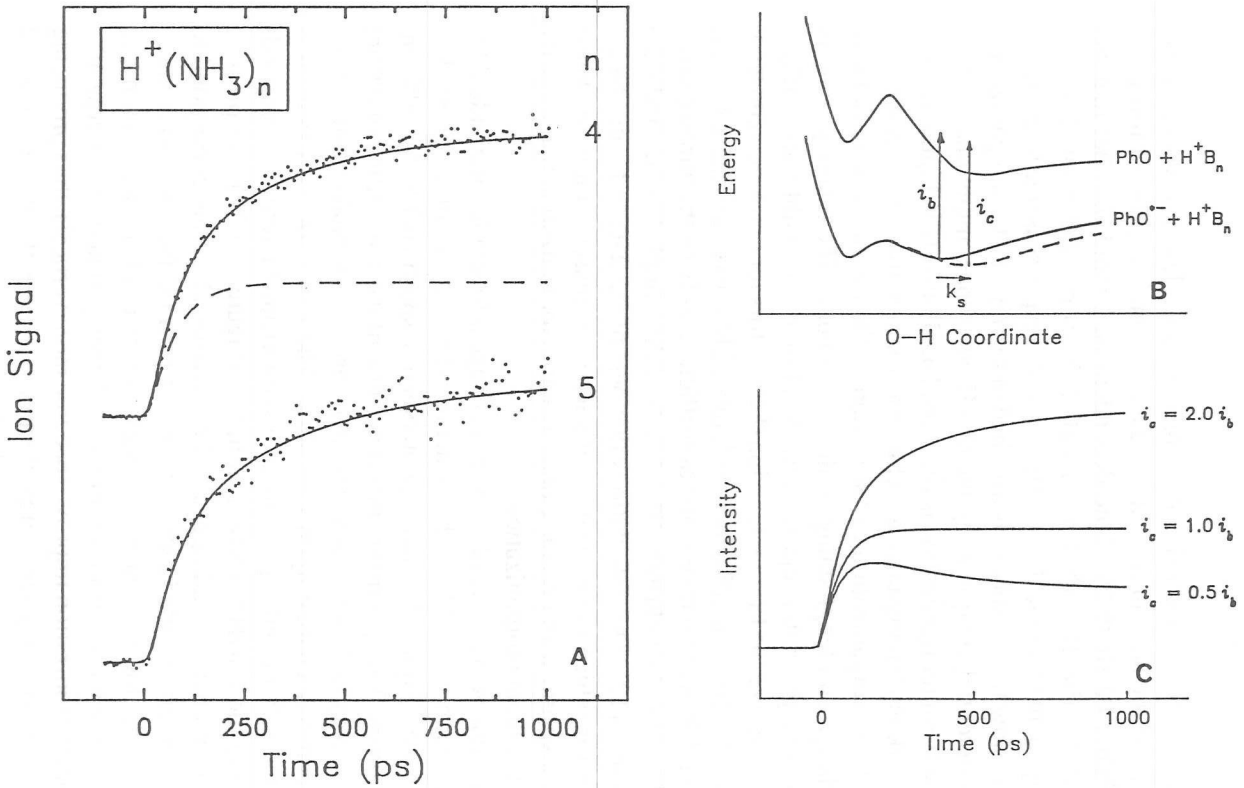

Fig. 6. (a) ESPT product formation kinetics (as measured by H^+B_n detection) for NH_3 solvation using 266-nm pump and 532-nm probe excitation. The data were fitted according to [12] for $k = (65\ \text{ps})^{-1}$, $k_s = (350\ \text{ps})^{-1}$, $i_c/i_b = 2.4$ (for $n = 4$); and $k = (65\ \text{ps})^{-1}$, $k_s = (300\ \text{ps})^{-1}$, $i_c/i_b = 2.0$ (for $n = 5$). Evaporation in the dissociative ionization process accounts for formation kinetics appearing at $n = 4$ despite reaction threshold at $n = 5$. (b) Schematic representation of the evolving solvent-relaxed ion-pair potential. The dotted line is a portrayal of the O—H potential for a relaxed solvent coordinate. (c) Time dependence calculated for $k = (65\ \text{ps})^{-1}$, $k_s = (300\ \text{ps})^{-1}$ and different ratios of unrelaxed (i_b) to relaxed (i_c) ionization efficiencies.

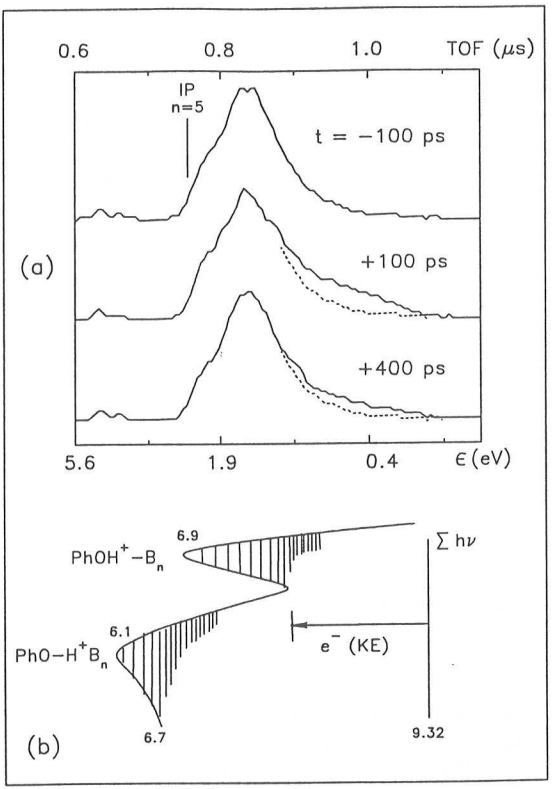

Fig. 7. (a) Time-resolved photoelectron spectra as a function of pump-probe delay time t (low resolution using 5 V acceleration). The $t = -100$ ps spectrum is superimposed on the latter two spectra (dashed line) to emphasize the low energy band. (b) Cluster ion potential energy curve along the O—H coordinate for $B_n = (NH_3)_5$ (energy values in eV, [13]).

The time dependence for the low-energy and high-energy photoelectron bands is plotted in Figure 8. The low-energy band (high-energy ions) increases rapidly in intensity and then decays at a slower rate. The high-energy band (low-energy ions) shows a corresponding slow rate of increase. A number of observations support the interpretation of a Franck-Condon distribution that changes with time due to solvent reorganization. The direction of the shift is from high-energy to low-energy ion excitation (red-shifted transitions to the ion), as expected for solvent relaxation. The low-energy band decays to a plateau level rather than to the baseline suggesting a spectral shift that is less than the width of the band. The high-energy band should grow from a similar non-zero baseline at $t < 0$, however, this level is obscured by the one-color background signal. The calculated curves in Figure 8 are based on a simple model that assumes a Gaussian photoelectron band that shifts to a new

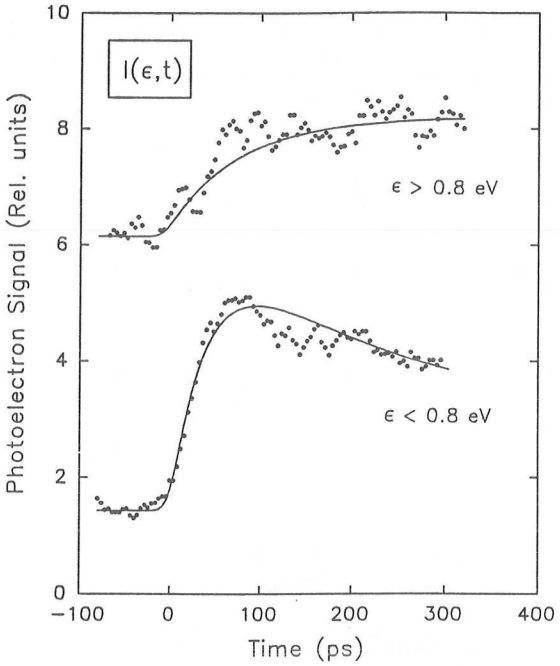

Fig. 8. Time-dependence of low-energy ($0.8 > \varepsilon > 0$ eV) and high-energy ($2.6 > \varepsilon > 0.8$ eV) photoelectron bands. Fitted curves were calculated for rate constants $k = (50\ \text{ps})^{-1}$ and $k_s = (300\ \text{ps})^{-1}$ and spectral parameters discussed in [13].

peak energy by a single-exponential rate constant k_s [13]. At this preliminary stage, the fits are not quantitative; however, the rate constants $k = (50\ \text{ps})^{-1}$ and $k_s = (300\ \text{ps})^{-1}$, used to fit the data, are in excellent agreement with the time-resolved mass spectrometry results in Figure 6a.

4. Free Radical Chemistry in Clusters

Free radical chemistry is usually associated with energetic chemistry (e.g., combustion, propulsion), but it is also important in the natural environment (e.g., atmospheric chemistry). The relationship between free radical chemistry in the gas phase and the condensed phase has attracted intense interest lately since the discovery that Antarctic stratospheric ozone depletion is aggravated by heterogeneous chemistry occuring on ice crystals [51]. Similarly, tropospheric pollution chemistry proceeds differently in the gas phase versus in aqueous aerosols. For example, the reaction of the common pollutant NO_2 with water to form nitric acid is endothermic in the gas-phase, but reacts efficiently in the aqueous phase. In water, the reaction is second order in NO_2 [52]; however, the kinetics may be different in small clusters.

Understanding this difference could explain the uptake of NO_2 in aqueous aerosols (in clouds and humid air) and its role in forming acid rain. We are beginning studies to measure atmospherically relevant chemistry in clusters. Another area where we are applying cluster research is in efforts to improve the efficiency of chemical propulsion. Rocket thrusters typically use cryogenic propellants (e.g., liquid H_2, O_2) or room temperature liquid propellants (e.g., hydrazines, hydrocarbons, N_2O_4) that are injected into a combustion chamber where they are assumed to volatilize before reacting. In fact, for many thruster designs, there is a growing suspicion that substantial chemistry occurs at the gas-liquid interface, which can adversely affect chemical thrust performance. One can find many examples in nature of chemistry occuring at gas-liquid interfaces. Studies of these chemistries in clusters could very well provide crucial understanding of the correspondence between gas-phase and condensed-phase chemical properties.

4.1 Methyl Radical Reaction in $(CH_3I)_n$ Clusters

In this section we give an example of a time-resolved study of radical chemistry in $(CH_3I)_n$ clusters where a combustion process is believed to have been initiated [19]. The chemistry is assumed to be driven by the exothermicity of the reaction

$$CH_3I + CH_3I \longrightarrow C_2H_6 + I_2 \qquad \Delta H = -0.52\ \text{eV}$$

A bottle of CH_3I clearly does not combust so one can safely conclude that the activation energy for the above reaction is very high. However, the reaction can be initiated by a radical mechanism that provides enough heat to sustain thermal chemistry. The cluster photoreactions were initiated by exciting into the directly dissociative $\tilde{A}$ state. The monomer reaction dissociates into CH_3 + I in less than 1 ps [53], however for certain cluster sizes one can expect sufficient caging of the initially formed radicals to induce chemistry within the cluster. Vaida *et al.* suggested that I_2 is produced in $(CH_3I)_n$ clusters on the basis of the detection of I_2^+ following nanosecond resonance ionization through the valence $\tilde{A}$ state [54]. These results, however, did not distinguish between I_2^+ formed by ionization of neutral product I_2 versus dissociation of cluster ions. To definitely establish the neutral cluster reaction channels, we identified the purely ionic fragmentation processes by employing direct variable-energy electron-impact (EI) ionization, and by recording size-specific cluster ion photodissociation mass spectra [7, 19, 25]. Since our work, two other studies of $(CH_3I)_n$ cluster chemistry have confirmed the neutral I_2 mechanism [55, 56].

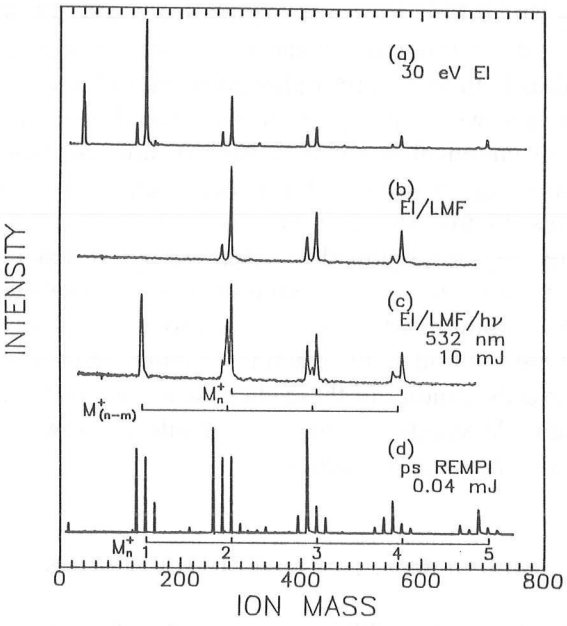

Fig. 9. $(CH_3I)_n$ cluster ionization mass spectra (M = CH_3I). (a) Direct ionization by EI excitation at 30 eV. (b) EI ionization and low mass filter (LMF). (c) Same, but with resonant photodissociation of cluster ions. (d) Picosecond $\tilde{A}$ state REMPI.

4.2 Neutral versus Ionic Cluster Reactions

When using resonance ionization to study photodissociation processes, the question often arises whether the detected fragment ions occur by ionization of neutral products or dissociation of parent ions. This competition is a concern in cluster research because the weak van der Waals (vdW) bonds usually mean that both neutral and ionic dissociation will occur. Picosecond pump-probe measurements help to sort out these competitive processes because they usually occur over different timescales. However, we also take the independent approach of measuring directly the ion dissociation mechanisms by EI ionization and by mass-selective ion photodissociation. The ion photodissociation experiments make use of a crossed electron-laser-molecular beam configuration as described in Section 2. The molecular clusters are first ionized by EI excitation, then mass filtered, and finally resonantly photodissociated using nanosecond laser pulses [7, 24, 25].

The methodology behind using both resonance ionization and direct ionization to identify neutral cluster reactions is illustrated in Figure 9 for $(CH_3I)_n$ clusters. EI ionization is used to ionize the clusters directly in order to ascertain fragment ions that occur exclusively by ion dissociation mechanisms.

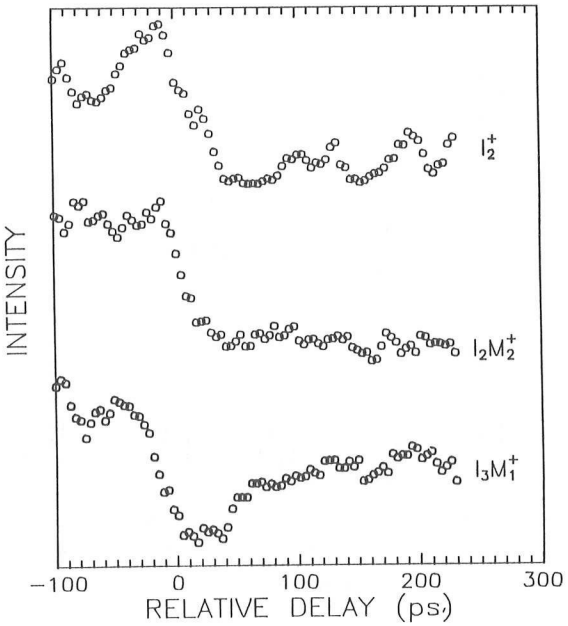

Fig. 10. Picosecond measurements using 266-nm pump and 532-nm probe: M_n (M = CH_3I) reaction for loss of two and three CH_3 groups [I_2M_{n-2} ($n = 2, 4$) and I_3M_{n-3} ($n = 4$), respectively].

The electron beam flux is sufficiently low that all excitation events occur by a single electron. The EI mass spectrum in Figure 9a shows that dissociation following cluster ionization consists only of C—I bond breaking or van der Waals (vdW) evaporation. The operation of the TOF low mass rejection filter is illustrated in Figure 9b where all masses less than the dimer mass are rejected from the excitation volume. (The details of this device are described elsewhere.) [7] In Figure 9c, the remaining ions are excited by a laser pulse that is resonant with a predissociative absorption in CH_3I. This excitation, which is known to cleave the C—I bond in monomer CH_3I^+ results only in vdW dissociation in the cluster ions. It is not surprising that the weakest bond breaks. (In Section 5.2 we present an example of a cluster ion dissociation in which a strong bond breaks preferentially to a weak bond.) Finally, Figure 9d contains the picosecond mass spectrum of $(CH_3I)_n$ resulting from excitation of the dissociative $\tilde{A}$ state. A distinctly different spectrum is observed from the ion fragmentation spectra in Figures 9a–c. As a result of the overall procedure encompassed by Figure 9, the additional signals in Figure 9d can be assigned to ionization of *neutral* reaction products.

The excited state neutral clusters undergo very rapid chemistry. Examples of picosecond pump-probe traces for some of the major products are given

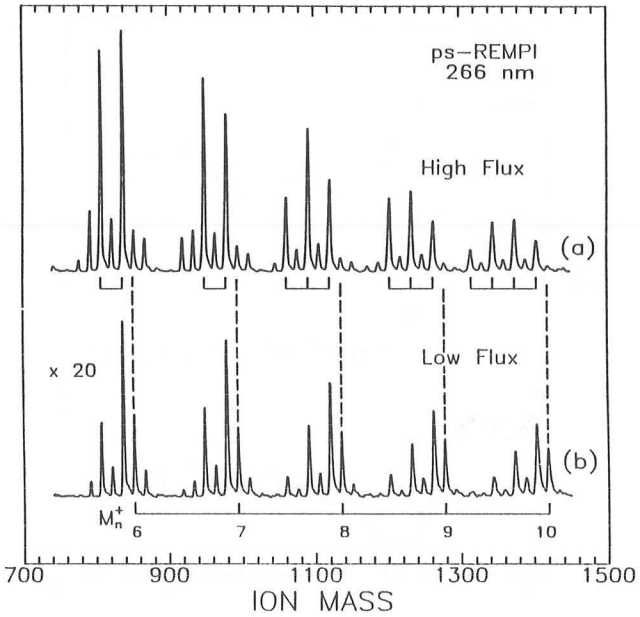

Fig. 11. ps-REMPI mass spectra showing reactions in larger clusters. The 266-nm high and low photon flux conditions differ by about a factor of three (within the range of 10^{27}–10^{28} cm^{-2} s^{-1}). The scaling factor in (b) shows that the overall signal intensity is steeply dependent on photon flux, however, the relative intensities are much less sensitive.

in Figure 10. A more complete mapping of the product time dependence versus cluster size has been reported elsewhere [19]. The main conclusion is that the chemistry is complex and that sequential processes indicative of a chain reaction appear to be occuring on the timescale of the 20–30 ps laser pulse durations. We explain only a few signals here. The measured rates for the formation of $I_2(CH_3I)_{n-2}$ as a function of cluster size n show a sharp decrease in signal level at $t = 0$ and remains constant to long delay times. The latter behavior suggests that photodissociation takes place in the long-lived ion, presumably due to the I_2 (or I_2^+) component. However the sharp threshold with delay time indicates that the ion, and therefore the neutral product, is formed within the instrument resolution of about 20 ps. Also shown in Figure 10 is the product $I_3(CH_3I)_{n-3}$, corresponding to loss of three CH_3 groups, that opens up for cluster sizes $n \geq 4$. The ion signal undergoes a rapid depletion at $t = 0$ within the instrument response time and then recovers for $t > 0$. Because of the signal recovery, it is unlikely that the dissociation occurs in the long-lived ion, but rather in the short-lived neutral. The $I_3M_{n-3}^+$ response is strong evidence for a neutral reaction mechanism.